INTERNATIONAL JOURNAL FOR NUMERICAL METHODS IN ENGINEERING
Int. J. Numer. Meth. Engng 2001; **50**:707–738

MITC finite elements for laminated composite plates

G. Alfano[1], F. Auricchio[2], L. Rosati[1,*,†] and E. Sacco[3]

[1] *Dip. di Scienza delle Costruzioni, Univ. dli. Napoli "Federico II", Italy*
[2] *Dip. di Meccanica Strutturale, Univ. di Pavia, Italy*
[3] *Dip. di Meccanica, Strutture, Territorio ed Ambiente, Univ. di Cassino, Italy*

SUMMARY

Within the framework of the first-order shear deformation theory, 4- and 9-node elements for the analysis of laminated composite plates are derived from the MITC family developed by Bathe and coworkers. To this end the bases of the MITC formulation are illustrated and suitably extended to incorporate the laminate theory. The proposed elements are locking-free, they do not have zero-energy modes and provide accurate in-plane deformations. Two consecutive regularizations of the extensional and flexural strain fields and the correction of the resulting out-of-plane stress profiles necessary to enforce exact fulfillment of the boundary conditions are shown to yield very satisfactory results in terms of transverse and normal stresses. The features of the proposed elements are assessed through several numerical examples, either for regular and highly distorted meshes. Comparisons with analytical solutions are also shown. Copyright © 2001 John Wiley & Sons, Ltd.

KEY WORDS: composites; plates; finite elements

1. INTRODUCTION

Fibre-reinforced composite plates and shells are finding an increasing interest in engineering applications. Consequently, efficient and robust computational tools are required for the analysis of such structural models. As a matter of fact, a large amount of laminate finite elements have been developed and incorporated in most commercial codes for structural analysis.

Finite elements for the analysis of laminated composite plates have been derived by using different laminate theories proposed in the literature, see References [1, 2] and references cited therein; such theories are usually referred to as equivalent single layer (ESL), layerwise and three dimensional.

In the context of the ESL theory, the simplest one is the classical laminate theory (CLT) which neglects the shear deformation in the laminate thickness. However, flat structures made of

*Correspondence to: L. Rosati, Dipartimento di Scienza delle Costruzioni, Università di Napoli "Federico II", Via Claudio 21, 80124 Napoli, Italy
†E-mail: rosati@unina.it

Contract/grant sponsor: National Council of Research (CNR)
Contract/grant sponsor: Italian Ministry of University and Research (MURST)

Received 22 February 1999
Revised 9 March 2000

fibre-reinforced composite materials are characterized by non-negligible shear deformations in the thickness since the longitudinal elastic modulus is much higher than the shear and the transversal moduli; hence the use of a shear deformation laminate theory is recommended. The extension of the Reissner [3] and Mindlin [4] model to the case of laminated anisotropic plates is known as first-order shear-deformation theory (FSDT) [5, 6], and accounts for the shear deformation in the thickness in the simplest way. This approach gives satisfactory results for a wide class of structural problems, even for moderately thick laminates; moreover, due to computational efficiency, it is currently used in large-scale computations typical of industrial applications.

More sophisticated laminate theories are the layerwise ones [7]. They lead to accurate results, especially for very thick laminates [8–11] and are particularly useful for analysing local effects [12, 13]. On the other hand, finite element formulations for layerwise theories are expensive in terms of CPU time.

In other words the FSDT provides a good compromise between numerical accuracy and computational burden. In fact, a current research topic concerns the development of effective finite elements for laminated plates and shells, within the framework of the FSDT, which are able to properly describe the structural behaviour in terms of displacements and stresses. The present study is a contribution in this direction and refers to the case of laminated composite plates under the hypotheses of linear elasticity, small strains and displacements.

Two basic issues have to be properly addressed in the formulation of laminated plate elements based on the FSDT: locking and a satisfactory evaluation of the stresses.

Several locking-free plate and laminate elements based on the FSDT have been proposed in the literature. The first elements exploited the selective reduced integration within a displacement formulation [14, 15]. This approach, equivalent to some special mixed formulations [16], presents however pathologies like spurious zero-energy modes [17]. Additional plate and laminate elements are based on mixed formulations obtained by adding internal modes to interpolate the stress resultants and to enhance the kinematic fields [18, 19]. Excellent numerical performances are then achieved at the expense of an increased computational burden. For instance, in References [18, 19] locking is avoided by introducing four internal bubble modes for the rotation field, four internal linear modes interpolating the shear forces and special *linked* shape functions relating the transverse displacement field to the nodal rotations.

In the FSDT, the issue concerning the evaluation of the stresses presents two separate aspects. Actually, while the computation of the in-plane stresses can be generally considered as satisfactory, the recovery of the out-of-plane transverse and normal stresses represents a critical aspect, although this usually occurs also for more refined ESL higher-order and layerwise theories. In fact, the constitutive law provides unacceptable layerwise constant values for the transverse shear stresses and would leave the out-of-plane normal stress undefined. Accurate values of the transverse shear stresses as well as of the out-of-plane normal stress are recovered only by using the three-dimensional differential equilibrium equations [20]. Accordingly, second and third derivatives of the displacement and rotation fields are required, a circumstance which usually leads to lack of accuracy in finite element models since interpolation functions do not satisfy the required continuity conditions. To overcome this difficulty the *enhanced modes* technique [21] has been successfully employed in Reference [19] to derive a 4-node laminated finite element. This technique provided good results in terms of shear stresses calculated by a direct use of the equilibrium equation, but resulted in an increase of computational effort.

In this paper we address the family of MITC elements (mixed interpolated tensorial components) proposed in References [22–24], since it leads to a very effective solution procedure for

homogeneous plates. An extension of the MITC plate elements to the case of composite laminates has been first proposed in Reference [25]. Herein we present 4- and 9-node composite laminated MITC plate elements with an investigation on their numerical performances.

In particular a new procedure is proposed for the evaluation of the out-of-plane stresses. It is based on a regularization of the extensional and flexural strain fields obtained by projecting onto the space of continuous fields, through a least-square technique [15], the finite element solution typically discontinuous at the interelement boundary.

Specifically, one regularization procedure is sufficient to provide satisfactory values of the transverse shear stresses while a further projection of the derivatives of the extensional and flexural strains is necessary to evaluate the out-of-plane normal stresses.

The outline of the paper is as follows. In Section 2 the first-order shear-deformation theory for composite laminated plates is recalled in a form suitable for the ensuing developments. Then the derivation of the out-of-plane stresses via the differential equilibrium equations is addressed in Section 3. The variational derivation of the MITC elements and their implementation are outlined in Section 4 while the post-processing procedure for recovering the out-of-plane stresses from the finite element solution is illustrated in Section 5. Numerical results are presented in Section 6; they show the good convergence properties of the MITC laminate elements as well as the excellent accuracy entailed by the proposed procedure in terms of the out-of-plane stresses. In particular accuracy turns out to be comparable with the one obtained by integrating the equilibrium equations for the exact two-dimensional solution of the FSDT. In this respect we remind that, for moderately thick plates, the transverse and the normal out-of-plane stresses evaluated in this way are in good agreement with the exact three-dimensional solution.

In order to simplify the notation we will assume throughout the paper that Greek indices range between 1 and 2, indices i and j range between 1 and 3 and that summation must be performed on repeated indices, unless otherwise specified.

2. FIRST-ORDER LAMINATE THEORY (FSDT)

Let us consider a laminated composite plate defined by

$$\mathscr{V} = \{(x_1, x_2, x_3) \in \mathscr{R}^3 / x_3 \in (-h/2, h/2),\ (x_1, x_2) \in \Omega \subset \mathscr{R}^2\} \tag{1}$$

where x_i are the co-ordinates with respect to an orthonormal basis $\{\mathbf{e}_i\}$, h is the thickness and Ω denotes the undeformed mid-plane identified by the intersection between $\mathscr{V}$ and the plane $x_3 = 0$.

The laminate is made up of n_l layers; the bottom and top surfaces of the kth one are, respectively, defined by the two vertical abscissas x_3^k and x_3^{k+1}, being $x_3^1 = -h/2$ and $x_3^{n_l+1} = h/2$.

Distributed transverse loads q_3^- and q_3^+ as well as distributed tangential loads q_α^- and q_α^+ can be applied on the bottom $(-)$ and top $(+)$ surfaces of the plate.

2.1. The FSDT model

The First-order Shear Deformation Theory, originally presented in References [3, 4] for homogeneous plates and in References [5, 6] for laminated composites, is based on the following assumptions [26]:

(i) the transverse strain component ε_{33} is zero;
(ii) the transverse shear strain components $\varepsilon_{\alpha 3}$ are constant in the thickness, that is $\varepsilon_{\alpha 3,3} = 0$;

(iii) the out-of-plane normal stress σ_{33} is zero;
(iv) the shear stresses $\sigma_{\alpha 3}$ are continuous piecewise quadratic functions of the x_3 coordinate,

where the comma stands for differentiation.

A rational deduction of the FSDT for homogeneous laminated plates has been presented in Reference [27] where it has been shown that the assumptions (i)–(iv) can be regarded as constraints on the strain and stress fields. Hence, rational derivations of plate or laminate theories can be obtained in the framework of the constrained elasticity.

The assumptions (i)–(ii), written in terms of displacement components s_i give

$$\begin{aligned} s_{3,3} &= 0 \\ s_{\alpha,33} + s_{3,\alpha 3} &= 0 \end{aligned} \tag{2}$$

respectively. By integrating relations (2) with respect to x_3, the following classical parametric representation of the displacement field is recovered:

$$\begin{aligned} s_1(x_1,x_2,x_3) &= u_1(x_1,x_2) + x_3\phi_1(x_1,x_2) \\ s_2(x_1,x_2,x_3) &= u_2(x_1,x_2) + x_3\phi_2(x_1,x_2) \\ s_3(x_1,x_2,x_3) &= u_3(x_1,x_2) \end{aligned} \tag{3}$$

Hence, the motion of each fibre orthogonal to the mid-plane is completely defined by the in-plane displacement components u_α, the transverse displacement u_3 and the rotation components ϕ_α.

According to Equations (3) the strain tensor can be decomposed as

$$\varepsilon_{ij} = e_{ij} + x_3\chi_{ij} + \gamma_{ij} \tag{4}$$

being e_{ij} the extensional strain, χ_{ij} the curvature and γ_{ij} the transverse shear strains, respectively, given by

$$[e_{ij}] = \begin{bmatrix} u_{1,1} & (u_{1,2}+u_{2,1})/2 & 0 \\ (u_{1,2}+u_{2,1})/2 & u_{2,2} & 0 \\ 0 & 0 & 0 \end{bmatrix} \tag{5}$$

$$[\chi_{ij}] = \begin{bmatrix} \phi_{1,1} & (\phi_{1,2}+\phi_{2,1})/2 & 0 \\ (\phi_{1,2}+\phi_{2,1})/2 & \phi_{2,2} & 0 \\ 0 & 0 & 0 \end{bmatrix} \tag{6}$$

$$[\gamma_{ij}] = \begin{bmatrix} 0 & 0 & (u_{3,1}+\phi_1)/2 \\ 0 & 0 & (u_{3,2}+\phi_2)/2 \\ (u_{3,1}+\phi_1)/2 & (u_{3,2}+\phi_2)/2 & 0 \end{bmatrix} \tag{7}$$

The elastic relation between the in-plane strains $\varepsilon_{\alpha\beta}$ and stresses $\sigma_{\alpha\beta}$ for the kth layer is

$$\sigma^k_{\alpha\beta} = \mathscr{C}^k_{\alpha\beta\gamma\delta}(e_{\gamma\delta} + x_3\chi_{\gamma\delta}) \tag{8}$$

where $\mathscr{C}^k$ is the fourth-order reduced elastic tensor obtained enforcing hypothesis (iii).

By integrating the constitutive relation (8) through the thickness we get

$$\begin{bmatrix} \mathbf{N} \\ \mathbf{M} \end{bmatrix} = \begin{bmatrix} \mathbf{A} & \mathbf{B} \\ \mathbf{B} & \mathbf{D} \end{bmatrix} \begin{bmatrix} \mathbf{e} \\ \boldsymbol{\chi} \end{bmatrix} \tag{9}$$

where $\mathbf{N}$ and $\mathbf{M}$ are the stress resultants defined by

$$N_{\alpha\beta} = \int_{-h/2}^{h/2} \sigma_{\alpha\beta}(x_3)\,\mathrm{d}x_3, \quad M_{\alpha\beta} = \int_{-h/2}^{h/2} x_3\sigma_{\alpha\beta}(x_3)\,\mathrm{d}x_3 \tag{10}$$

and the fourth-order constitutive tensors $\mathbf{A}$, $\mathbf{B}$ and $\mathbf{D}$ are given by

$$\begin{aligned} A_{\alpha\beta\gamma\delta} &= \sum_{k=1}^{n_l} \left(x_3^{k+1} - x_3^k\right) C^k_{\alpha\beta\gamma\delta} \\ B_{\alpha\beta\gamma\delta} &= \frac{1}{2} \sum_{k=1}^{n_l} \left[\left(x_3^{k+1}\right)^2 - \left(x_3^k\right)^2\right] C^k_{\alpha\beta\gamma\delta} \\ D_{\alpha\beta\gamma\delta} &= \frac{1}{3} \sum_{k=1}^{n_l} \left[\left(x_3^{k+1}\right)^3 - \left(x_3^k\right)^3\right] C^k_{\alpha\beta\gamma\delta} \end{aligned} \tag{11}$$

The tensor $\mathbf{B}$ accounts for the coupling between extension and bending; it vanishes for symmetric laminates.

In plate or laminate FSDT, the relation between the resultant shear forces, defined as

$$Q_\alpha = \int_{-h/2}^{h/2} \sigma_{\alpha 3}(x_3)\,\mathrm{d}x_3 \tag{12}$$

and the shear strains $\gamma_{\alpha 3}$ is affected by the so-called shear correction factors. In fact, the shear stiffness $\mathbf{H}$, given by

$$H_{\alpha\beta} = \sum_{k=1}^{n_l} (x_3^{k+1} - x_3^k) C^k_{\alpha 3\beta 3} \tag{13}$$

must be corrected by the fourth-order tensor $\boldsymbol{\kappa}$ defined as

$$\boldsymbol{\kappa} = \kappa_{\alpha\beta}\mathbf{d}_\alpha \boxtimes \mathbf{d}_\beta \tag{14}$$

where

$$\mathbf{d}_1 = \begin{bmatrix} 1 & 0 \\ 0 & 0 \end{bmatrix}, \quad \mathbf{d}_2 = \begin{bmatrix} 0 & 0 \\ 0 & 1 \end{bmatrix} \tag{15}$$

and the tensorial product $\boxtimes$ between second-order tensors is defined by: $(\mathbf{a}\boxtimes\mathbf{b})\mathbf{c} = \mathbf{a}\mathbf{c}\mathbf{b}^{\mathrm{t}}$, being $\mathbf{a}$, $\mathbf{b}$ and $\mathbf{c}$ arbitrary second-order tensors. Finally, the relation between $\mathbf{Q}$ and $\boldsymbol{\gamma}$ is written in the form

$$\mathbf{Q} = \tilde{\mathbf{H}}\boldsymbol{\gamma} \quad \text{with } \tilde{\mathbf{H}} = \boldsymbol{\kappa}\mathbf{H} \tag{16}$$

We emphasize that the presence of the shear factors is due to assumption (iv) on the shear stress profile in the laminate thickness.

In fact, according to hypothesis (iv) the shear stress can be represented in the form

$$\sigma_{\alpha 3}(x_1, x_2, x_3) = g_\alpha(x_3) Q_\alpha(x_1, x_2) \tag{17}$$

where $g_\alpha(x_3)$ is a piecewise quadratic shape function defining the shear stress profile in the thickness. The shear strain energy computed in the whole thickness of the laminate is

$$\mathscr{E} = \frac{1}{2} \int_{-h/2}^{h/2} \sigma_{\alpha 3} \gamma_{\alpha 3} \, \mathrm{d}x_3 \tag{18}$$

Since $\gamma_{\alpha 3}$ is constant in the thickness, taking into account relations (12) and (16), Equation (18) is written as

$$\mathscr{E} = \tfrac{1}{2} Q_\alpha \gamma_{\alpha 3} = \tfrac{1}{2} (\tilde{H}^{-1})_{\alpha\beta} \, Q_\alpha Q_\beta \tag{19}$$

On the other hand, recalling position (17), the complementary shear strain energy in the thickness is

$$\begin{aligned} \mathscr{E}^* &= \frac{1}{2} \int_{-h/2}^{h/2} \sigma_{\alpha 3} \mathscr{S}_{\alpha 3 \beta 3} \sigma_{\beta 3} \, \mathrm{d}x_3 \\ &= \frac{1}{2} \left[\int_{-h/2}^{h/2} g_\alpha \mathscr{S}_{\alpha 3 \beta 3} g_\beta \, \mathrm{d}x_3 \right] Q_\alpha Q_\beta \end{aligned} \tag{20}$$

where $\mathscr{S} = \mathscr{C}^{-1}$ is the compliance tensor of the typical lamina.

By enforcing the equality between expressions (19) and (20) it results

$$(\tilde{H}^{-1})_{\alpha\beta} = \int_{-h/2}^{h/2} g_\alpha \mathscr{S}_{\alpha 3 \beta 3} g_\beta \, \mathrm{d}x_3 \quad \text{no sum} \tag{21}$$

Thus, the shear correction factors $\kappa_{\alpha\beta}$ depends on the shape functions g_α and g_β. If x_1 and x_2 are principal material directions of orthotropy, i.e. $\mathscr{S}_{1323} = 0$ and $\tilde{H}_{12} = 0$, Equation (21) gives

$$\frac{1}{\kappa_{\alpha\alpha} H_{\alpha\alpha}} = \int_{-h/2}^{h/2} \frac{1}{\mathscr{C}_{\alpha 3 \alpha 3}} (g_\alpha)^2 \, \mathrm{d}x_3 \quad \text{no sum} \tag{22}$$

and hence, explicitly, it is

$$\kappa_{\alpha\alpha} = \frac{1}{H_{\alpha\alpha}} \int_{-h/2}^{h/2} \frac{(g_\alpha)^2}{\mathscr{C}_{\alpha 3 \alpha 3}} \, \mathrm{d}x_3 \quad \text{no sum} \tag{23}$$

The shear factors represent an additional unknown of the problem, since the shear profile g_α is not known *a priori* for composite laminates. The common choice $\kappa_{11} = \kappa_{22} = \frac{5}{6}$ and $\kappa_{12} = 0$ is correct only for homogeneous plates; conversely for laminated plates it is usually adopted as a starting value, to be used in an iterative predictor-corrector procedure, as suggested in References [19, 28].

2.2. Displacement-based variational formulations

The total potential energy functional for the laminate FSDT model is given by

$$\begin{aligned}\mathscr{F}(\mathbf{u},u_3,\boldsymbol{\phi}) = &\frac{1}{2}\int_\Omega \mathbf{A}\nabla^{\mathrm{s}}\mathbf{u}\cdot\nabla^{\mathrm{s}}\mathbf{u}\,\mathrm{d}\Omega + \int_\Omega \mathbf{B}\nabla^{\mathrm{s}}\mathbf{u}\cdot\nabla^{\mathrm{s}}\boldsymbol{\phi}\,\mathrm{d}\Omega \\ &+ \frac{1}{2}\int_\Omega \mathbf{D}\nabla^{\mathrm{s}}\boldsymbol{\phi}\cdot\nabla^{\mathrm{s}}\boldsymbol{\phi}\,\mathrm{d}\Omega \\ &+ \frac{1}{2}\int_\Omega \tilde{\mathbf{H}}(\nabla u_3+\boldsymbol{\phi})\cdot(\nabla u_3+\boldsymbol{\phi})\,\mathrm{d}\Omega - \mathscr{F}_{\mathrm{ext}}(\mathbf{u},u_3,\boldsymbol{\phi})\end{aligned} \tag{24}$$

where the external load potential is

$$\begin{aligned}\mathscr{F}_{\mathrm{ext}}(\mathbf{u},u_3,\boldsymbol{\phi}) = &\int_\Omega (q_3^- + q_3^+)u_3\,\mathrm{d}\Omega + \int_\Omega (q_\alpha^- + q_\alpha^+)u_\alpha\,\mathrm{d}\Omega \\ &+ \int_\Omega \frac{h}{2}(q_\alpha^+ - q_\alpha^-)\phi_\alpha\,\mathrm{d}\Omega + \mathscr{F}_{\mathrm{bou}}\end{aligned} \tag{25}$$

The term $\mathscr{F}_{\mathrm{bou}}$ accounts for the boundary conditions on $\partial\Omega$. The vectors $\mathbf{u}$ and $\boldsymbol{\phi}$ collect the in-plane displacement and rotation components u_α and ϕ_α while the symbol ∇^{s} indicates the symmetric part of the gradient operator.

The field and boundary equations for the FSDT are then obtained as stationary conditions for $\mathscr{F}$. In particular, by making use of Equations (9) and (16) the following differential field equations

$$\begin{aligned} N_{\alpha\beta,\beta} + q_\alpha^- + q_\alpha^+ &= 0, \quad Q_{\alpha,\alpha} + q_3^- + q_3^+ = 0 \\ M_{\alpha\beta,\beta} + \frac{h}{2}(q_\alpha^+ - q_\alpha^-) &= Q_\alpha \end{aligned} \tag{26}$$

are fulfilled by the exact solution of the boundary value problem.

3. RECOVERING OF THE OUT-OF-PLANE STRESSES

The solution provided by the FSDT does not directly provide the out-of-plane stresses, that is the transverse shear stress components σ_{13} and σ_{23} and the normal stress σ_{33}.

In fact the constitutive elastic law of the composite laminate would provide unacceptable values of the transverse shear stresses, while the component σ_{33} would remain undefined.

For this reason it is common practice to recover the out-of-plane stress by using the three-dimensional equilibrium equations. In the absence of body forces, they read

$$\sigma_{ij,j}^k = 0, \quad i,j = 1,2,3, \;\; k = 1,2,\ldots,n_l \tag{27}$$

where the in-plane components $\sigma_{\alpha\beta}^k$ in the kth layer are related to the extensional and flexural strains $\mathbf{e}$ and $\boldsymbol{\chi}$ through the elastic law (8).

3.1. The transverse shear stresses

Starting from Equation (27) ($i=1,2$) and making use of Equation (8), we get the following recursive expression for the transverse shear stresses $\sigma^k_{\alpha 3}$ in the kth layer:

$$\sigma^k_{\alpha 3}(x_3)=\sigma^{k-1}_{\alpha 3}(x^k_3)-\int_{x^k_3}^{x_3} C^k_{\alpha\beta\gamma\delta}(e_{\gamma\delta,\beta}+\xi_3\chi_{\gamma\delta,\beta})\,\mathrm{d}\xi_3, \quad k=1,2,\ldots,n_l \tag{28}$$

supplemented by the n_l equilibrium conditions

$$\sigma^0_{\alpha 3}(x^1_3)=-q^-_\alpha, \quad \sigma^k_{\alpha 3}(x^k_3)=\sigma^{k-1}_{\alpha 3}(x^k_3), \quad k=2,\ldots,n_l \tag{29}$$

With a slight abuse of notation we have denoted by $\sigma^0_{\alpha 3}(x^1_3)$ the value of the component $\sigma_{\alpha 3}$ at the bottom face of the plate, i.e. $\sigma^0_{\alpha 3}(x^1_3)=\sigma^1_{\alpha 3}(-h/2)$.

Notice that in this section, for brevity, the explicit dependence of the functions upon the in-plane co-ordinates x_1 and x_2 is omitted.

By computing the integrals in Equation (28) we get

$$\sigma^k_{\alpha 3}(x_3)=\sigma^{k-1}_{\alpha 3}(x^k_3)-C^k_{\alpha\beta\gamma\delta}\left[(x_3-x^k_3)e_{\gamma\delta,\beta}+\frac{(x_3)^2-(x^k_3)^2}{2}\chi_{\gamma\delta,\beta}\right], \quad k=1,\ldots,n_l \tag{30}$$

The further condition $\sigma^{n_l}_{\alpha 3}(h/2)=q^+_\alpha$ is dependent upon the ones in (29). Actually the value $\sigma^{n_l}_{\alpha 3}(h/2)$ is given by

$$\begin{aligned}\sigma^{n_l}_{\alpha 3}(h/2)&=-q^-_\alpha-\left(\int_{-h/2}^{h/2} C_{\alpha\beta\gamma\delta}\,\mathrm{d}\xi_3\right)e_{\gamma\delta,\beta}-\left(\int_{-h/2}^{h/2}\xi_3 C_{\alpha\beta\gamma\delta}\,\mathrm{d}\xi_3\right)\chi_{\gamma\delta,\beta}\\&=-q^-_\alpha-\left(A_{\alpha\beta\gamma\delta}e_{\gamma\delta}+B_{\alpha\beta\gamma\delta}\chi_{\gamma\delta}\right)_{,\beta}=-q^-_\alpha-N_{\alpha\beta,\beta}=q^+_\alpha\end{aligned} \tag{31}$$

The last equality follows from relations (26).

Equilibrium condition (12) is exactly satisfied too. Actually, an integration by parts (28) yields

$$\begin{aligned}\int_{-h/2}^{h/2}\sigma_{\alpha 3}(x_3)\,\mathrm{d}x_3&=\int_{-h/2}^{h/2}\left[-q^-_\alpha-\int_{-h/2}^{x_3}C_{\alpha\beta\gamma\delta}(e_{\gamma\delta,\beta}+\xi_3\chi_{\gamma\delta,\beta})\,\mathrm{d}\xi_3\right]\mathrm{d}x_3\\&=-q^-_\alpha h-\left[x_3\int_{-h/2}^{x_3}C_{\alpha\beta\gamma\delta}(e_{\gamma\delta,\beta}+\xi_3\chi_{\gamma\delta,\beta})\mathrm{d}\xi_3\right]_{-h/2}^{h/2}\\&\quad+\int_{-h/2}^{h/2}C_{\alpha\beta\gamma\delta}\,x_3(e_{\gamma\delta,\beta}+x_3\chi_{\gamma\delta,\beta})\,\mathrm{d}x_3\\&=-q^-_\alpha h-\frac{h}{2}\left[\left(\int_{-h/2}^{h/2}C_{\alpha\beta\gamma\delta}\,\mathrm{d}x_3\right)e_{\gamma\delta}+\left(\int_{-h/2}^{h/2}x_3C_{\alpha\beta\gamma\delta}\,\mathrm{d}x_3\right)\chi_{\gamma\delta}\right]_{,\beta}\\&\quad+\left[\left(\int_{-h/2}^{h/2}x_3C_{\alpha\beta\gamma\delta}\,\mathrm{d}x_3\right)e_{\gamma\delta}+\left(\int_{-h/2}^{h/2}x_3^2C_{\alpha\beta\gamma\delta}\,\mathrm{d}x_3\right)\chi_{\gamma\delta}\right]_{,\beta}\\&=-q^-_\alpha h-N_{\alpha\beta,\beta}\frac{h}{2}+M_{\alpha\beta,\beta}\end{aligned} \tag{32}$$

From Equations $(26)_3$ we then deduce

$$\int_{-h/2}^{h/2} \sigma_{\alpha 3}(x_3)\,\mathrm{d}x_3 = M_{\alpha\beta,\beta} + (q_\alpha^+ - q_\alpha^-)\frac{h}{2} = Q_\alpha \tag{33}$$

In order to get the explicit expression of the transverse shear stresses as function of the in-plane displacement and rotation fields, we substitute relations (5) and (6) in Equation (30) to get

$$\sigma_{\alpha 3}^k(x_3) = \sigma_{\alpha 3}^{k-1}(x_3^k) - \left[C_{\alpha\beta\gamma\delta}^k (x_3 - x_3^k) \left(\frac{u_{\gamma,\delta\beta} + u_{\delta,\gamma\beta}}{2} \right) + \frac{x_3^2 - (x_3^k)^2}{2} \left(\frac{\phi_{\gamma,\delta\beta} + \phi_{\delta,\gamma\beta}}{2} \right) \right], \quad k = 1, \ldots, n_l \tag{34}$$

where $\sigma_{\alpha 3}^0(x_3^1) = -q_\alpha^-$.

3.2. The out-of-plane normal stresses

Equation (27), for $i = 3$, provides the following expression of the stress component σ_{33} as a function of the out-of-plane components σ_{13} and σ_{23}:

$$\sigma_{33}^k(x_3) = \sigma_{33}^{k-1}(x_3^k) - \int_{x_3^k}^{x_3} \sigma_{\alpha 3,\alpha}(\xi_3)\,\mathrm{d}\xi_3, \quad k = 1, \ldots, n_l \tag{35}$$

where the n_l equilibrium conditions

$$\sigma_{33}^0(x_3^1) = -q_3^-, \quad \sigma_{33}^k(x_3^k) = \sigma_{33}^{k-1}(x_3^k), \quad k = 2, \ldots, n_l \tag{36}$$

have to be taken into account and $\sigma_{33}^0(x_3^1)$ denotes the value of σ_{33} at the bottom face of the plate.

By substituting Equation (30) into Equation (35) we get

$$\sigma_{33}^k(x_3) = \sigma_{33}^{k-1}(x_3^k) + c^k(x_3 - x_3^k) + C_{\alpha\beta\gamma\delta}^k \left[\frac{(x_3 - x_3^k)^2}{2} e_{\gamma\delta,\alpha\beta} + \frac{x_3^3 - 3(x_3^k)^2 x_3 + 2(x_3^k)^3}{6} \chi_{\gamma\delta,\alpha\beta} \right], \quad k = 1, \ldots, n_l \tag{37}$$

The n_l integration constants c^k can be evaluated by the relation

$$c^k = \sigma_{33,3}^k(x_3^k) = -\sigma_{\alpha 3,\alpha}^k(x_3^k)$$

Actually, since the conditions $\sigma_{\alpha 3}^0(x_3^1) = -q_\alpha^-$ and $\sigma_{\alpha 3}^k(x_3^k) = \sigma_{\alpha 3}^{k-1}(x_3^k)$ hold for any x_1 and x_2, it turns out to be $\sigma_{\alpha 3,\alpha}^0(x_3^1) = -q_{\alpha,\alpha}^-$ and $\sigma_{\alpha 3,\alpha}^k(x_3^k) = \sigma_{\alpha 3,\alpha}^{k-1}(x_3^k)$. Hence $\sigma_{33,3}^1(x_3^1) = q_{\alpha,\alpha}^-$ and $\sigma_{33,3}^k(x_3^k) = \sigma_{33,3}^{k-1}(x_3^k)$, so that

$$\begin{aligned} c^1 &= q_{\alpha,\alpha}^- \\ c^k &= c^{k-1} + C_{\alpha\beta\gamma\delta}^{k-1} \left[(x_3^k - x_3^{k-1}) e_{\gamma\delta,\alpha\beta} + \frac{(x_3^k)^2 - (x_3^{k-1})^2}{2} \chi_{\gamma\delta,\alpha\beta} \right], \quad k = 2, \ldots, n_l \end{aligned} \tag{38}$$

The further conditions $\sigma_{33}^{n_l}(h/2) = q_3^+$ and $\sigma_{33,3}^{n_l}(h/2) = -q_{\alpha,\alpha}^+$ are dependent upon the ones in (36) and (38). Actually

$$\begin{aligned}\sigma_{33}^{n_l}(h/2) &= -q_3^- - \int_{-h/2}^{h/2} \sigma_{\alpha 3,\alpha}(\xi_3)\,\mathrm{d}\,\xi_3 = -q_3^- - \left(\int_{-h/2}^{h/2} \sigma_{\alpha 3}(\xi_3)\,\mathrm{d}\,\xi_3\right)_{,\alpha} \\ &= -q_3^- - Q_{\alpha,\alpha} = q_3^+\end{aligned} \tag{39}$$

while, by making use of Equation (31), we obtain

$$\sigma_{33,3}^{n_l}(h/2) = -\sigma_{\alpha 3,3}^{n_l}(h/2) = q_{\alpha,\alpha}^- + N_{\alpha\beta,\alpha\beta} = -q_{\alpha,\alpha}^+ \tag{40}$$

Notice again that the last identities in the previous two equations follow from Equation (26) since we are considering the exact solution of the two-dimensional problem.

Finally, substituting relations Equations (5) and (6) into formulas (37) and (38) we get the expression depending upon the in-plane displacement and rotation fields:

$$\begin{aligned} c^k &= c^{k-1} + C_{\alpha\beta\gamma\delta}^{k-1}\left[\left(x_3^k - x_3^{k-1}\right)\left(\frac{u_{\gamma,\delta\beta\alpha} + u_{\delta,\gamma\beta\alpha}}{2}\right)\right. \\ &\quad \left. + \frac{\left(x_3^k\right)^2 - \left(x_3^{k-1}\right)^2}{2}\left(\frac{\phi_{\gamma,\delta\beta\alpha} + \phi_{\delta,\gamma\beta\alpha}}{2}\right)\right] \\ \sigma_{33}^k\left(x_3\right) &= \sigma_{33}^{k-1}\left(x_3^k\right) + c^k\left(x_3 - x_3^k\right) \\ &\quad + C_{\alpha\beta\gamma\delta}^k\left[\frac{\left(x_3 - x_3^k\right)^2}{2}\left(\frac{u_{\gamma,\delta\beta\alpha} + u_{\delta,\gamma\beta\alpha}}{2}\right)\right. \\ &\quad \left. + \frac{x_3^3 - 3\left(x_3^k\right)^2 x_3 + 2\left(x_3^k\right)^3}{6}\left(\frac{\phi_{\gamma,\delta\beta\alpha} + \phi_{\delta,\gamma\beta\alpha}}{2}\right)\right] \end{aligned} \tag{41}$$

for each $k = 1, \ldots, n_l$, where $\sigma_{33}^0(x_3^1) = -q_3^-$ and $c^1 = q_{\alpha,\alpha}^-$.

4. THE MITC 4- AND 9-NODE LAMINATED PLATE ELEMENTS

The MITC family of plates and shell elements has been conceived by Bathe and coworkers [22–24] as a refined tool to satisfy the usual isotropy and convergence requirements of finite element formulations [15]. In particular the MITC elements are locking-free, do not contain any spurious zero-energy modes and have a good predictive capability for displacements, bending moments and membrane forces.

Further, they are relatively insensitive to element distorsions and have been deeply investigated from the theoretical point of view; in fact their convergence properties have been mathematically analyzed in Reference [29].

In spite of the acronymous MITC, which stands for *mixed interpolation of tensorial components*, the formulation does not require any additional parameter with respect to the strictly necessary

kinematical nodal ones. Hence, for a plate element belonging to the MITC family, the number of element parameters is equal to $5n_e$, where n_e is the number of nodes per element.

An extension of the MITC plate elements to the case of composite laminates has been first proposed in Reference [25]. In-plane displacement components must be introduced as additional kinematic parameters and the laminate constitutive equations (9) and (16) must be used in place of the corresponding ones for the homogenous plate.

The variational framework is still represented by the extremum principle for the total potential energy (25) and the key idea of the MITC approach consists in interpolating the transverse shear strain field differently from the one which can be derived from the displacement and rotation fields via Equation (8).

For the sake of completeness the basic elements of such treatment are addressed for a 4- and 9-node composite laminated plate element and, with a view towards computer implementation, the related formulas are detailed.

The finite element equations for the proposed MITC formulation are derived as stationary conditions for the discretized form of the following functional (25):

$$\begin{aligned}\mathscr{F}_{\text{ept}}^{\text{MITC}}(\mathbf{u}^d, u_3^d, \boldsymbol{\phi}^d) = {} & \frac{1}{2}\int_\Omega \mathbf{A}\nabla^{\text{s}}\mathbf{u}^d \cdot \nabla^{\text{s}}\mathbf{u}^d \,\mathrm{d}\Omega + \int_\Omega \mathbf{B}\nabla^{\text{s}}\mathbf{u}^d \cdot \nabla^{\text{s}}\boldsymbol{\phi}^d \,\mathrm{d}\Omega \\ & + \frac{1}{2}\int_\Omega \mathbf{D}\nabla^{\text{s}}\boldsymbol{\phi}^d \cdot \nabla^{\text{s}}\boldsymbol{\phi}^d \,\mathrm{d}\Omega \\ & + \frac{1}{2}\int_\Omega \tilde{\mathbf{H}}\boldsymbol{\gamma}(\nabla u_3^d, \boldsymbol{\phi}^d)\cdot\boldsymbol{\gamma}(\nabla u_3^d, \boldsymbol{\phi}^d)\,\mathrm{d}\Omega - \mathscr{F}_{\text{ext}}(\mathbf{u}^d, u_3^d, \boldsymbol{\phi}^d)\end{aligned} \tag{42}$$

where the apex ^{d} refers to interpolated fields and denotes a characteristic size of the finite element discretization.

The interpolated fields u_α^d, u_3^d and ϕ_α^d are given in each element by

$$\begin{aligned} u_\alpha^d(x_1,x_2) &= \Xi^n(x_1,x_2)u_\alpha^n, \quad u_3^d(x_1,x_2) = \Xi^n(x_1,x_2)u_3^n \\ \phi_\alpha^d(x_1,x_2) &= \Xi^n(x_1,x_2)\phi_\alpha^n \quad n = 1,\ldots,n_e \end{aligned} \tag{43}$$

where u_α^n, u_3^n, ϕ_α^n denote the numerical parameters and Ξ^n the shape function pertaining to the nth node.

The transverse shear strains $\gamma_{\alpha 3}$ in Equation (42) are evaluated from a suitable interpolation of the covariant components $\tilde{\gamma}_{\alpha 3}$ exactly computed from u_3^d and ϕ_α^d via Equation (7) in a set of n_t *tying* points.

The covariant basis $\{\mathbf{g}_\alpha\}$ at the tth tying point is assumed as

$$(\mathbf{g}_\alpha)_\beta = \frac{\partial x_\beta}{\partial r_\alpha} \tag{44}$$

where r_α is the αth local co-ordinate in the reference domain. In a local co-ordinate system $\mathbf{r} = (r_1, r_2)$, the covariant components of the trasverse shear strains are then given by

$$\tilde{\gamma}_{\alpha 3}(\mathbf{r}) = (\mathbf{g}_\alpha)_\beta(\mathbf{r})\gamma_{\beta 3}(\mathbf{r}) = J_{\beta\alpha}(\mathbf{r})\gamma_{\beta 3}(\mathbf{r}) \tag{45}$$

where $\mathbf{J}(\mathbf{r})$ is the jacobian of the isoparametric mapping evaluated at the point $\mathbf{r}$.

The values of $\tilde{\gamma}^t_{\alpha 3}$ at the tth tying point, of local co-ordinates $\mathbf{r}^t$, are then computed as follows:

$$\tilde{\gamma}^t_{\alpha 3} = \sum_{n=1}^{n_e} J_{\beta\alpha}(\mathbf{r}^t)(\Xi^n_{,\beta}(\mathbf{r}^t)u^n_3 + \Xi^n(\mathbf{r}^t)\phi^n_\beta) = \sum_{n=1}^{n_e} W^{nt}_\alpha u^n_3 + Z^{nt}_{\alpha\beta}\phi^n_\beta \tag{46}$$

where

$$W^{nt}_\alpha = J_{\beta\alpha}(\mathbf{r}^t)\Xi^n_{,\beta}(\mathbf{r}^t), \quad Z^{nt}_{\alpha\beta} = J_{\beta\alpha}(\mathbf{r}^t)\Xi^n(\mathbf{r}^t) \tag{47}$$

and the summation has been now denoted explicitly.

The values $\tilde{\gamma}^t_{\alpha 3}$ are then interpolated in natural co-ordinates by means of n_t shape functions ψ^t_α

$$\tilde{\gamma}_{\alpha 3}(\mathbf{r}) = \sum_{t=1}^{n_t} \psi^t_\alpha(\mathbf{r})\tilde{\gamma}^t_{\alpha 3} = \sum_{n=1}^{n_e}[(\tilde{B}^n_{sw})_\alpha(\mathbf{r})u^n_3 + (\tilde{B}^n_{s\phi})_{\alpha\beta}(\mathbf{r})\phi^n_\beta] \quad \text{(no sum on } \alpha) \tag{48}$$

The matrices $\tilde{\mathbf{B}}^n_{sw}$ and $\tilde{\mathbf{B}}^n_{s\phi}$ have, respectively, dimensions 2×1 and 2×2 and provide the covariant representation of the transverse shear strain field as a function of the kinematic parameters u^n_3 and $\boldsymbol{\phi}^n$ pertaining to the nth node of the element. Their expressions can be obtained by substituting Equation (46) into Equation (48):

$$(\tilde{B}^n_{sw})_\alpha(\mathbf{r}) = \sum_{t=1}^{n_t} \psi^t_\alpha(\mathbf{r})W^{nt}_\alpha, \quad (\tilde{B}^n_{s\phi})_{\alpha\beta}(\mathbf{r}) = \sum_{t=1}^{n_t} \psi^t_\alpha(\mathbf{r})Z^{nt}_{\alpha\beta} \quad \text{(no sum on } \alpha) \tag{49}$$

The relevant expressions of the matrices $\mathbf{B}^n_{sw}$ and $\mathbf{B}^n_{s\phi}$, which are associated with the interpolation of the cartesian representation $\gamma_{\alpha 3}$, are obtained by inverting relations (45):

$$\mathbf{B}^n_{sw}(\mathbf{r}) = [\mathbf{J}^t(\mathbf{r})]^{-1}\tilde{\mathbf{B}}^n_{sw}(\mathbf{r}), \quad \mathbf{B}^n_{s\phi}(\mathbf{r}) = [\mathbf{J}^t(\mathbf{r})]^{-1}\tilde{\mathbf{B}}^n_{s\phi}(\mathbf{r}) \tag{50}$$

For the 4- and 9-node elements 2 and 6 tying points have been used, respectively, for each shear strain component.

The shape functions ψ^t_α for the 4-node element are

$$\psi^1_1 = \tfrac{1}{2}(1 + r_2), \quad \psi^1_2 = \tfrac{1}{2}(1 + r_1)$$
$$\psi^2_1 = \tfrac{1}{2}(1 - r_2), \quad \psi^2_2 = \tfrac{1}{2}(1 - r_1)$$

For the sake of completeness we also provide the expressions of the shape functions for the 9-node element since they were not explicitly reported in the original paper [24]:

$$\psi^1_1(r_1, r_2) = \frac{1}{4}(1 + \sqrt{3}r_1)\left(1 + \frac{1}{\sqrt{0.6}}r_2\right) - \frac{1}{2}\psi^5_1(r_1, r_2)$$
$$\psi^2_1(r_1, r_2) = \frac{1}{4}(1 - \sqrt{3}r_1)\left(1 + \frac{1}{\sqrt{0.6}}r_2\right) - \frac{1}{2}\psi^6_1(r_1, r_2)$$

$$\psi_1^3(r_1,r_2)=\frac{1}{4}(1-\sqrt{3}r_1)\left(1-\frac{1}{\sqrt{0.6}}r_2\right)-\frac{1}{2}\psi_1^6(r_1,r_2)$$

$$\psi_1^4(r_1,r_2)=\frac{1}{4}(1+\sqrt{3}r_1)\left(1-\frac{1}{\sqrt{0.6}}r_2\right)-\frac{1}{2}\psi_1^5(r_1,r_2)$$

$$\psi_1^5(r_1,r_2)=\frac{1}{2}(1+\sqrt{3}r_1)\left[1-\left(\frac{1}{\sqrt{0.6}}r_2\right)^2\right]$$

$$\psi_1^6(r_1,r_2)=\frac{1}{2}(1-\sqrt{3}r_1)\left[1-\left(\frac{1}{\sqrt{0.6}}r_2\right)^2\right]$$

and

$$\psi_2^1(r_1,r_2)=\frac{1}{4}\left(1+\frac{1}{\sqrt{0.6}}r_1\right)(1+\sqrt{3}r_2)-\frac{1}{2}\psi_2^5(r_1,r_2)$$

$$\psi_2^2(r_1,r_2)=\frac{1}{4}\left(1-\frac{1}{\sqrt{0.6}}r_1\right)(1+\sqrt{3}r_2)-\frac{1}{2}\psi_2^5(r_1,r_2)$$

$$\psi_2^3(r_1,r_2)=\frac{1}{4}\left(1-\frac{1}{\sqrt{0.6}}r_1\right)(1-\sqrt{3}r_2)-\frac{1}{2}\psi_2^6(r_1,r_2)$$

$$\psi_2^4(r_1,r_2)=\frac{1}{4}\left(1+\frac{1}{\sqrt{0.6}}r_1\right)(1-\sqrt{3}r_2)-\frac{1}{2}\psi_2^6(r_1,r_2)$$

$$\psi_2^5(r_1,r_2)=\frac{1}{2}\left[1-\left(\frac{1}{\sqrt{0.6}}r_1\right)^2\right](1+\sqrt{3}r_2)$$

$$\psi_2^6(r_1,r_2)=\frac{1}{2}\left[1-\left(\frac{1}{\sqrt{0.6}}r_1\right)^2\right](1-\sqrt{3}r_2)$$

For further details the reader is referred to the original papers [22–24].

5. RECOVERING OF THE OUT-OF-PLANE STRESS FROM THE FINITE ELEMENT SOLUTION

Formulas (34) and (41) require, respectively, the evaluation of the second and third derivatives of the in-plane displacement and rotation fields. Hence they cannot be used for the MITC elements, as well as for all the finite element formulations which ensure continuity of the displacement and rotation fields only up to their first derivatives.

A first way to address this problem clearly amounts to developing a kinematically richer laminated plate element, so as to improve the accuracy of the derivatives required by Equations (34) and (41). This approach has been exploited in Reference [19] to evaluate the transverse shear stresses.

In this paper we propose a different strategy which consists in evaluating the values $e_{\gamma\delta,\beta}$ and $\chi_{\gamma\delta,\beta}$ from two regularized fields $(\overline{e_{\gamma\delta}})$ and $(\overline{\chi_{\gamma\delta}})$ and, in turn, the values $e_{\gamma\delta,\alpha\beta}$ and $\chi_{\gamma\delta,\alpha\beta}$ from two additional regularized fields $(\overline{\overline{e_{\gamma\delta,\beta}}})$ and $(\overline{\overline{\chi_{\gamma\delta,\beta}}})$.

The fulfillment of the boundary conditions for the out-of-plane stresses evaluated, via Equations (34) and (41), as function of the regularized fields is then enforced through two suitable correction procedures detailed in the sequel.

5.1. *Regularization of the extensional and bending strain fields*

The regularized fields are obtained by using the projection procedure which is usually adopted in the stress smoothing preliminary to plotting or in the numerical estimate of the error in finite element solutions. To this end we denote by $L^2(\Omega)$ the linear space of square integrable functions.

In particular, the fields $(\overline{e_{\gamma\delta}})$ and $(\overline{\chi_{\gamma\delta}})$ are the orthogonal projections in the norm of $L^2(\Omega)$ of the fields $e^{\mathrm{fe}}_{\gamma\delta}$ and $\chi^{\mathrm{fe}}_{\gamma\delta}$, computed from the finite element solution via Equation (5), onto the subspace $\mathscr{V}_d$ collecting the element-wise polynomial functions interpolating the nodal values $(\overline{e_{\gamma\delta}})^n$ and $(\overline{\chi_{\gamma\delta}})^n$.

They are then computed by the relations:

$$(\overline{e_{\gamma\delta}})(x_1,x_2)=\Xi^n(x_1,x_2)(\overline{e_{\gamma\delta}})^n, \qquad (\overline{\chi_{\gamma\delta}})(x_1,x_2)=\Xi^n(x_1,x_2)(\overline{\chi_{\gamma\delta}})^n \tag{51}$$

where Ξ^n is again the shape function pertaining to the nth node and the nodal values $(\overline{e_{\gamma\delta}})^n$ and $(\overline{\chi_{\gamma\delta}})^n$ are obtained by solving the standard least-square problems

$$\begin{aligned} &\min_{(\overline{e_{\gamma\delta}})^m}\int_\Omega \left[\Xi^m(x_1,x_2)(\overline{e_{\gamma\delta}})^m - e^{\mathrm{fe}}_{\gamma\delta}(x_1,x_2)\right]^2 \mathrm{d}\Omega \\ &\min_{(\overline{\chi_{\gamma\delta}})^m}\int_\Omega \left[\Xi^m(x_1,x_2)(\overline{\chi_{\gamma\delta}})^m - \chi^{\mathrm{fe}}_{\gamma\delta}(x_1,x_2)\right]^2 \mathrm{d}\Omega \end{aligned} \tag{52}$$

They yield in turn

$$(\overline{e_{\gamma\delta}})^n=P^{nm}(\bar{a}_{\gamma\delta})^m, \quad (\overline{\chi_{\gamma\delta}})^n=P^{nm}(\bar{b}_{\gamma\delta})^m \tag{53}$$

where

$$\begin{aligned} P^{nm}&=\int_\Omega \Xi^m(x_1,x_2)\Xi^n(x_1,x_2)\,\mathrm{d}\Omega \\ (\bar{a}_{\gamma\delta})^m&=\int_\Omega \Xi^m(x_1,x_2)e^{\mathrm{fe}}_{\gamma\delta}(x_1,x_2)\,\mathrm{d}\Omega, \quad (\bar{b}_{\gamma\delta})^m=\int_\Omega \Xi^m(x_1,x_2)\chi^{\mathrm{fe}}_{\gamma\delta}(x_1,x_2)\,\mathrm{d}\Omega \end{aligned} \tag{54}$$

In order to speed up the calculations, lumped approximations for the matrix $\mathbf{P}$ are usually adopted, see also Reference [15] for more details.

Analogously the two regularized fields $(\overline{\overline{e_{\gamma\delta,\beta}}})$ and $(\overline{\overline{\chi_{\gamma\delta,\beta}}})$ turn out to be the orthogonal projections, in the norm of $L^2(\Omega)$, of the fields $(\overline{e_{\gamma\delta}})_{,\beta}$ and $(\overline{\chi_{\gamma\delta}})_{,\beta}$ onto the subspace $\mathscr{V}_d$. They are then provided by the relations:

$$(\overline{\overline{e_{\gamma\delta,\beta}}})(x_1,x_2)=\Xi^n(x_1,x_2)(\overline{\overline{e_{\gamma\delta,\beta}}})^n, \quad (\overline{\overline{\chi_{\gamma\delta,\beta}}})(x_1,x_2)=\Xi^n(x_1,x_2)(\overline{\overline{\chi_{\gamma\delta,\beta}}})^n \tag{55}$$

where the nodal values $(\overline{\overline{e_{\gamma\delta,\beta}}})^n$ and $(\overline{\overline{\chi_{\gamma\delta,\beta}}})^n$ are given by

$$(\overline{\overline{e_{\gamma\delta,\beta}}})^n = P^{nm}(\overline{\overline{a}}_{\gamma\delta\beta})^m, \quad (\overline{\overline{\chi_{\gamma\delta,\beta}}})^n = P^{nm}(\overline{\overline{b}}_{\gamma\delta\beta})^m \tag{56}$$

In the above relations P^{nm} is still supplied by $(54)_1$ while $(\overline{\overline{a}}_{\gamma\delta\beta})^m$ and $(\overline{\overline{b}}_{\gamma\delta\beta})^m$ are now expressed as

$$(\overline{\overline{a}}_{\gamma\delta\beta})^m = \int_\Omega \Xi^m(x_1,x_2)(\overline{e_{\gamma\delta}})_{,\beta}(x_1,x_2)\,\mathrm{d}\Omega, \quad (\overline{\overline{b}}_{\gamma\delta\beta})^m = \int_\Omega \Xi^m(x_1,x_2)(\overline{\chi_{\gamma\delta}})_{,\beta}(x_1,x_2)\,\mathrm{d}\Omega \tag{57}$$

The evaluation of the transverse shear stresses can now be performed by substituting expressions (51) of the regularized fields $(\overline{e_{\gamma\delta}})$ and $(\overline{\chi_{\gamma\delta}})$ in place of $e_{\gamma\delta}$ and $\chi_{\gamma\delta}$ in Equation (30):

$$\sigma^k_{\alpha 3}(x_3) = \sigma^{k-1}_{\alpha 3}(x_3^k) + C^k_{\alpha\beta\gamma\delta}\sum_{n=1}^{n_e}\Xi^n_{,\beta}\left[(x_3 - x_3^k)(\overline{e_{\gamma\delta}})^n + \frac{x_3^2 - (x_3^k)^2}{2}(\overline{\chi_{\gamma\delta}})^n\right] \quad k = 1,\ldots,n_l \tag{58}$$

where we remind that $\sigma^0_{\alpha 3}(x_3^1) = -q^-_\alpha$.

Similarly, the out-of-plane normal stress is obtained by substituting expressions (55) of the twice regularized fields $(\overline{\overline{e_{\gamma\delta,\beta}}})$ and $(\overline{\overline{\chi_{\gamma\delta,\beta}}})$ in place of $e_{\gamma\delta,\beta}$ and $\chi_{\gamma\delta,\beta}$ in Equations (37) and (38):

$$\begin{aligned} c^k &= c^{k-1} + C^{k-1}_{\alpha\beta\gamma\delta}\sum_{n=1}^{n_e}\Xi^n_{,\alpha}\left[(x_3^k - x_3^{k-1})(\overline{\overline{e_{\gamma\delta,\beta}}})^n + \frac{(x_3^k)^2 - (x_3^{k-1})^2}{2}(\overline{\overline{\chi_{\gamma\delta,\beta}}})^n\right] \\ \sigma^k_{33}(x_3) &= \sigma^{k-1}_{33}(x_3^k) + c^k(x_3 - x_3^k) + C^k_{\alpha\beta\gamma\delta}\sum_{n=1}^{n_e}\Xi^n_{,\alpha}\left[\frac{(x_3 - x_3^k)^2}{2}(\overline{\overline{e_{\gamma\delta,\beta}}})^n\right. \\ &\quad \left. + \frac{x_3^3 - 3(x_3^k)^2x_3 + 2(x_3^k)^3}{6}(\overline{\overline{\chi_{\gamma\delta,\beta}}})^n\right] \end{aligned} \tag{59}$$

with the positions $\sigma^0_{33}(x_3^1) = -q_3^-$ and $c^1 = q^-_{\alpha,\alpha}$.

Remark 1. The overall procedure requires the additional storage of $18N_n$ nodal parameters, being N_n the number of nodes of the whole discretized structure. Actually, $6N_n$ parameters are needed for allocating the values $(\overline{e_{\gamma\delta}})^n$ and $(\overline{\chi_{\gamma\delta}})^n$, while $12N_n$ are required for the values $(\overline{\overline{e_{\gamma\delta,\beta}}})^n$ and $(\overline{\overline{\chi_{\gamma\delta,\beta}}})^n$.

5.2. A correction of the out-of-plane stress profiles

In general, due to the error which affects the finite element solution, relations (26) no longer hold. Accordingly, the conditions $\sigma^{n_l}_{\alpha 3}(h/2) = q^+_\alpha$, $\sigma^{n_l}_{33}(h/2) = q^+_3$ and $\sigma^{n_l}_{33,3}(h/2) = -q^+_{\alpha,\alpha}$ could not be exactly satisfied.

It is then necessary to correct the stress profiles, as shown in Reference [19] for the transverse shear stress. We thus propose a correction procedure for the shear stresses, slightly different with respect to the one presented in Reference [19], and a new one for the out-of-plane stress. Namely, denoting by $\sigma^{nc}_{\alpha 3}$ the non-corrected solution provided by Equation (58), we compute the corrected one $\sigma^c_{\alpha 3}$ by adding a second-degree polynomial function

$$\Delta\sigma_{\alpha 3}(x_3) = \sigma^c_{\alpha 3}(x_3) - \sigma^{nc}_{\alpha 3}(x_3) = a_0 + a_1\left(x_3 + \frac{h}{2}\right) + a_2\left(\frac{h^2}{4} - x_3^2\right) \tag{60}$$

which satisfies the three conditions

$$\Delta\sigma_{\alpha 3}(-h/2)=0, \quad \Delta\sigma_{\alpha 3}(h/2)=\Delta q_\alpha^+, \quad \int_{-h/2}^{h/2}\Delta\sigma_{\alpha 3}(x_3)\,\mathrm{d}x_3=\Delta Q_\alpha$$

where

$$\Delta q_\alpha^+ = q_\alpha^+ - \sigma_{\alpha 3}^{\mathrm{nc}}(h/2), \quad \Delta Q_\alpha = Q_\alpha - \int_{-h/2}^{h/2}\sigma_{\alpha 3}^{\mathrm{nc}}(x_3)\,\mathrm{d}x_3$$

We thus have

$$a_0=0, \quad a_1=\frac{\Delta q_\alpha^+}{h}, \quad a_2=\frac{6}{h^3}\left(\Delta Q_\alpha-\frac{\Delta q_\alpha^+ h}{2}\right) \tag{61}$$

Proceeding as above, we denote by $\sigma_{33}^{\mathrm{nc}}$ the non-corrected expression of out-of-plane normal stress, provided by (59), and by σ_{33}^{c} the corrected one. This is obtained by adding a third-degree polynomial function:

$$\Delta\sigma_{33}(x_3)=\sigma_{33}^{\mathrm{c}}(x_3)-\sigma_{33}^{\mathrm{nc}}(x_3)=b_0+b_1\left(x_3+\frac{h}{2}\right)+b_2\left(x_3+\frac{h}{2}\right)^2+b_3\left(x_3+\frac{h}{2}\right)^3 \tag{62}$$

which fulfills the four conditions

$$\Delta\sigma_{33}(-h/2)=0, \quad \Delta\sigma_{33,3}(-h/2)=0$$
$$\Delta\sigma_{33}(h/2)=\Delta q_3^+, \quad \Delta\sigma_{33,3}(h/2)=\Delta q_{\alpha,\alpha}^+$$

where

$$\Delta q_3^+ = q_3^+ - \sigma_{33}^{\mathrm{nc}}(h/2), \quad \Delta q_{\alpha,\alpha}^+ = -\left[q_{\alpha,\alpha}^+ + \sigma_{33,3}^{\mathrm{nc}}(h/2)\right]$$

In this way, the following values:

$$b_0=b_1=0, \quad b_2=\frac{3}{h^2}\Delta q_3^+-\frac{\Delta q_{\alpha,\alpha}^+}{h}, \quad b_3=-\frac{2}{h^3}\Delta q_3^+ + \frac{\Delta q_{\alpha,\alpha}^+}{h^2} \tag{63}$$

are obtained.

Some considerations, in addition to the ones already reported in Remark 1, are in order for what concerns the computational burden of the proposed procedure. In fact, each one of the postprocessing phases detailed above is operatively similar to the one currently employed for plotting fields which are discontinuous between elements; this is the case, for instance, of the stress field in a displacement-based finite element formulation.

Remark 2. Once the out-of-plane stresses have been recovered, the shear stress profile can be evaluated by using formula (17). As a consequence, updated values of the shear correction factors can be obtained through formula (21). Hence they can be used as starting values of the iterative technique presented in Reference [19] within the framework of a different plate element.

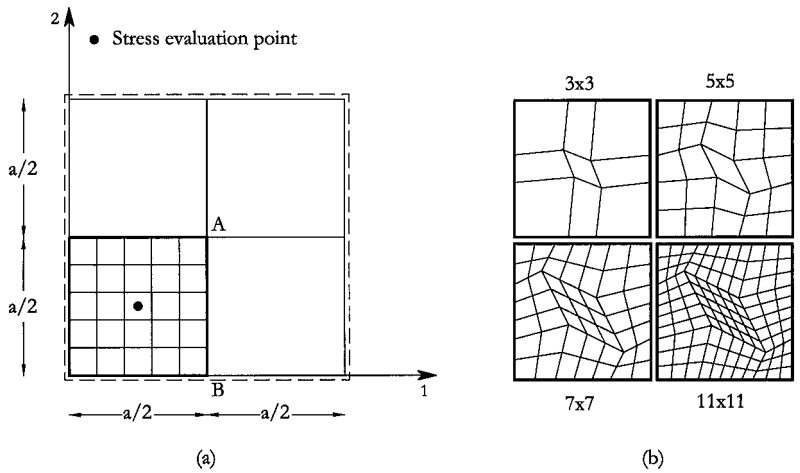

Figure 1. Simply supported plate: finite element meshes and geometric data: (a) regular mesh 5×5; (b) distorted meshes.

6. NUMERICAL RESULTS

The MITC laminate element formulation and the proposed strategy for recovering the out-of-plane stress components have been implemented in the finite element code FEAP (Finite Element Analysis Program) [15] and their numerical performances have been assessed by several applications.

Hereafter we report some results obtained for the benchmark problem of a simply supported square cross-ply laminated plate subjected to a sinusoidal transversal load with maximum value q. For symmetry reasons only a quarter of the plate has been discretized and the finite element meshes which have been adopted are illustrated in Figure 1.

Denoting by h and a the thickness and the width of the laminate, respectively, a constant value for the thickness-to-side ratio $h/a = 0.12$ is assumed. The examples refer to the layer sequences 0/90 and 0/90/0.

Each layer is characterized by the following mechanical properties: $E_L/E_T = 25$, $\nu = 0.25$, $G_{LT}/E_T = 0.5$, $G_{TT}/E_T = 0.2$, where L stands for longitudinal and T for transversal, characteristic of a high modulus orthotropic graphite/epoxy composite material.

In order to thoroughly investigate on the convergence properties of the laminated MITC elements, the relative error of the finite element solution is plotted in Figures 2–7 versus the number n of nodes per edge. For completeness we also report, in the log–log scale, the error which characterizes the element EML4 [19], based on a mixed formulation and the use of the enhanced modes. The relative error has been conventionally defined as the ratio $(u - u^*)/u^*$ where u is the value of a displacement component obtained in the finite element solution and u^* is the analogous quantity provided by the continuum FSDT theory [30]. Both u and u^* have been evaluated at a given point of the mesh as detailed hereafter.

Figures 2–5, 6 and 7 refer to the layer sequences 0/90 and 0/90/0, respectively. In particular Figures 2 and 3 show in turn the results concerning the vertical displacement of the mid-plate, see point A of Figure 1, for regular and distorted meshes. Analogously Figures 4 and 5 illustrate

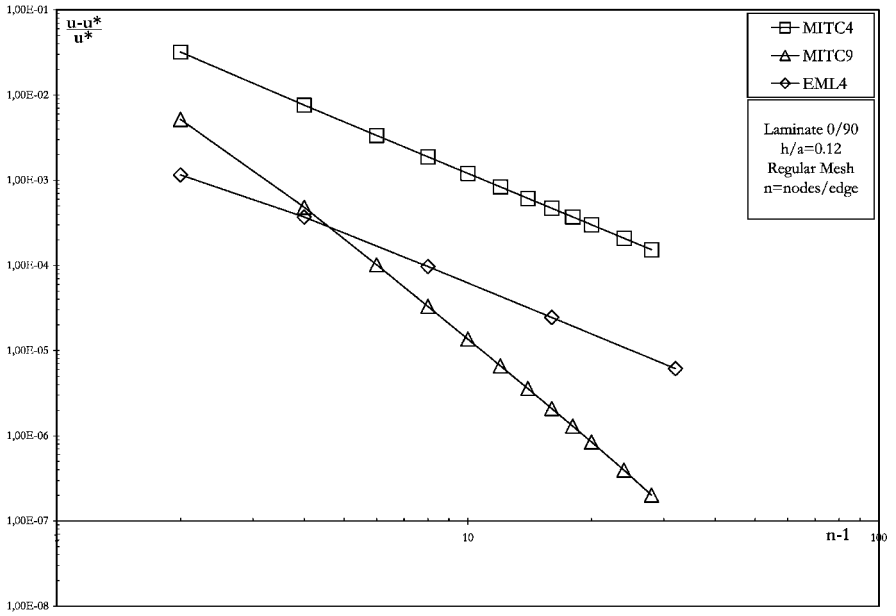

Figure 2. Convergence analysis for mid-plate vertical displacement (Point A)—regular mesh.

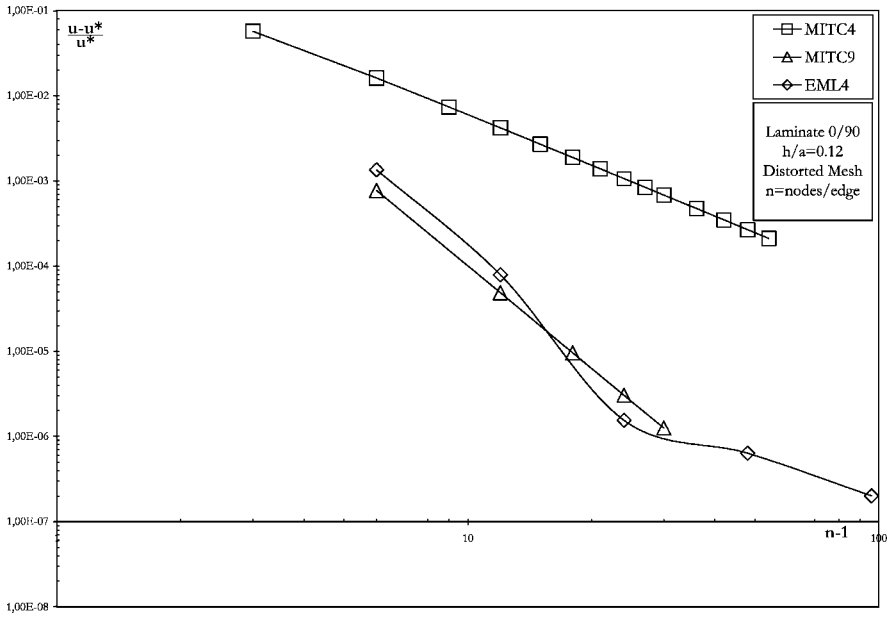

Figure 3. Convergence analysis for mid-plate vertical displacement (Point A)—distorted mesh.

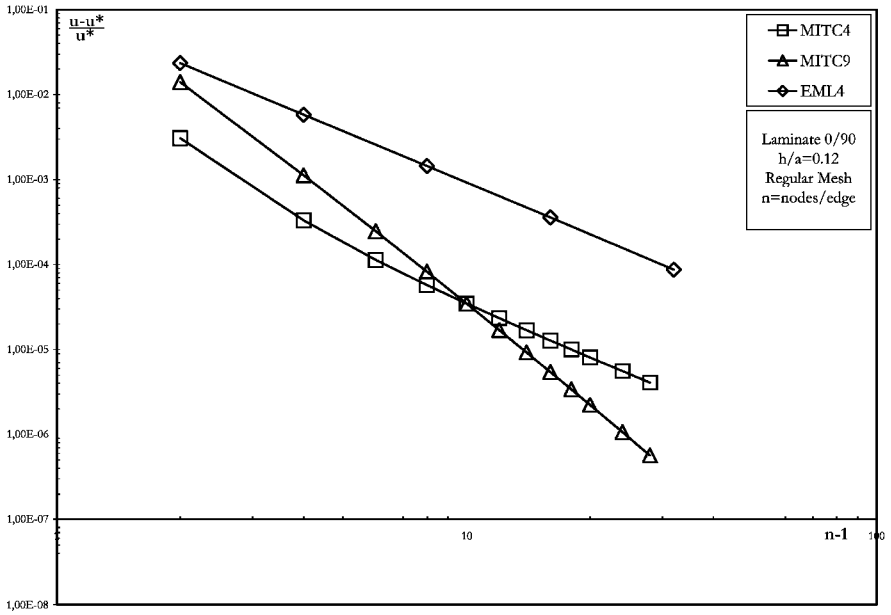

Figure 4. Convergence analysis for mid-side horizontal displacement (Point B)—regular mesh.

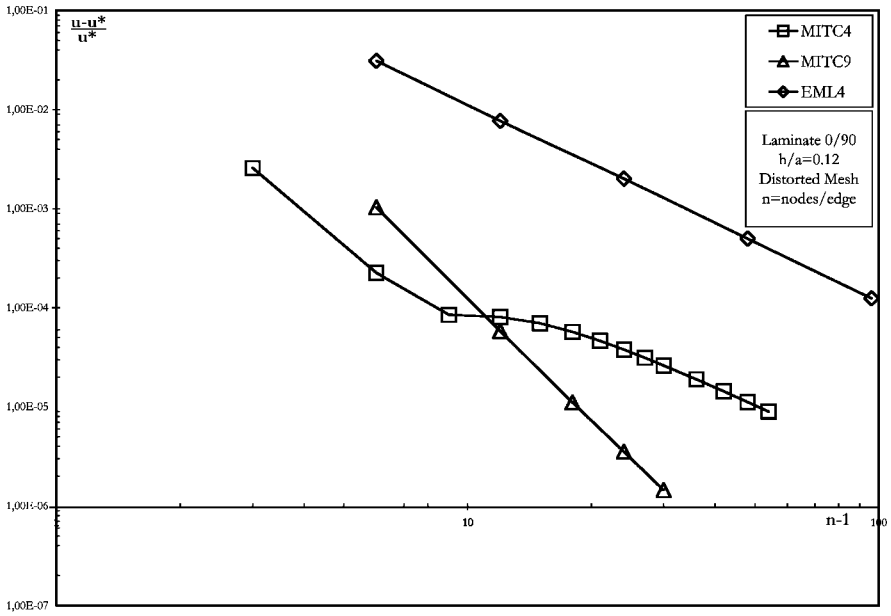

Figure 5. Convergence analysis for mid-side horizontal displacement (Point B)—distorted mesh.

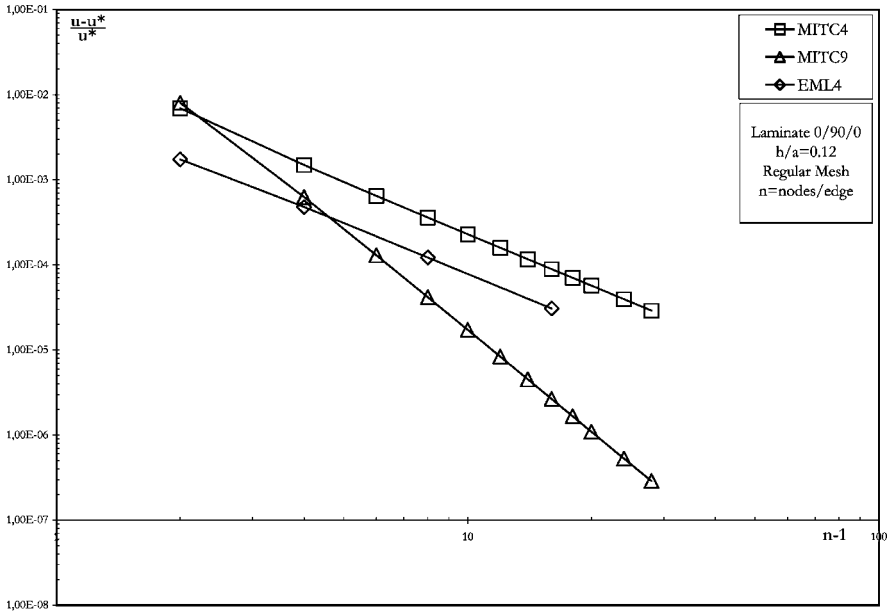

Figure 6. Convergence analysis for mid-plate vertical displacement (Point A)—regular mesh.

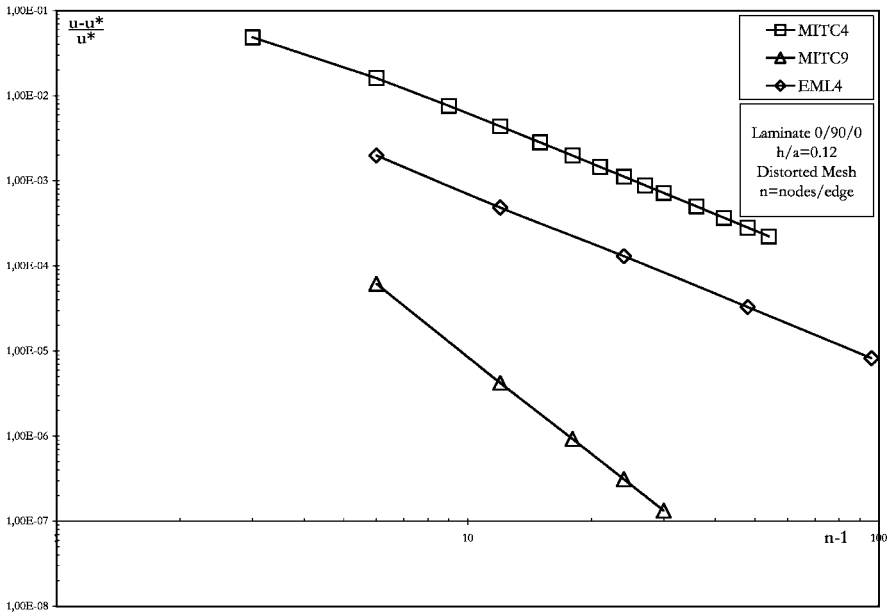

Figure 7. Convergence analysis for mid-plate vertical displacement (Point A)—distorted mesh.

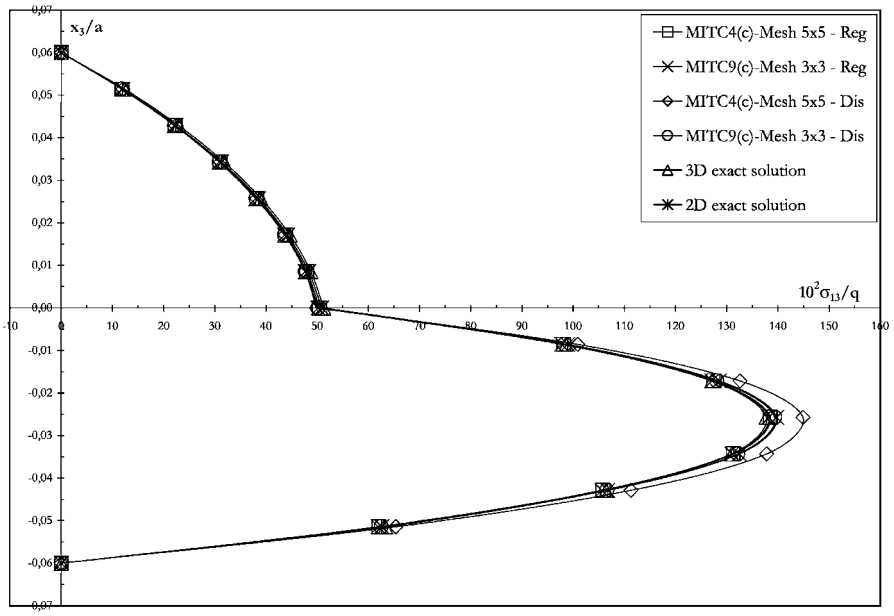

Figure 8. Through-the-thickness distributions of stress σ_{13} at $x = y = a/4$; Laminate 0/90.

the results in terms of the horizontal displacement of point B, see Figure 1, situated at the mid-side of the plate. Notice that non-linear diagrams in the log–log scale have been found only for lower-order elements, EML4 in Figure 3 and MITC4 in Figure 5, and for the severely distorted meshes considered in numerical simulations.

Figures 8–12 report the out-of-plane stress profiles, evaluated at the centre of the quarter of plate, versus the through-the-thickness adimensional abscissa x_3/a. The graphs refer to MITC4 and MITC9 elements for different meshes, both regular (reg) and distorted (dis), characterized by $n \times n$ number of elements. In particular we have considered coarse meshes characterized by $n = 5$ and 3 for the MITC4 and MITC9 elements, respectively. For completeness the closed-form solution obtained by a two-dimensional [30] and a three-dimensional [20] approach are also included.

The results have been obtained by applying the correction procedure outlined in Section 5; this is indicated through the abbreviation (c). It is apparent that very accurate results, close to the exact two-dimensional solutions, are obtained both for the out-of-plane shear stresses, see Figures 8–10, and normal stresses, Figures 11 and 12.

In order to investigate on the modification entailed by the correction procedure of the out-of-plane stress profiles resulting from the finite element solution, we report the corrected (c) and non-corrected (nc) profiles in the same graph. Specifically Figures 13 and 14 refer to the out-of-plane shear stress in the laminate 0/90 for regular and distorted meshes, respectively. Analogously, Figures 15–18 illustrate the results obtained for the shear stresses σ_{13} and σ_{23} with reference to the laminate 0/90/0. The importance of the correction procedure is also illustrated for the out-of-plane normal stress in Figures 19 and 20 and Figures 21 and 22 for the layer sequences 0/90 and 0/90/0, respectively.

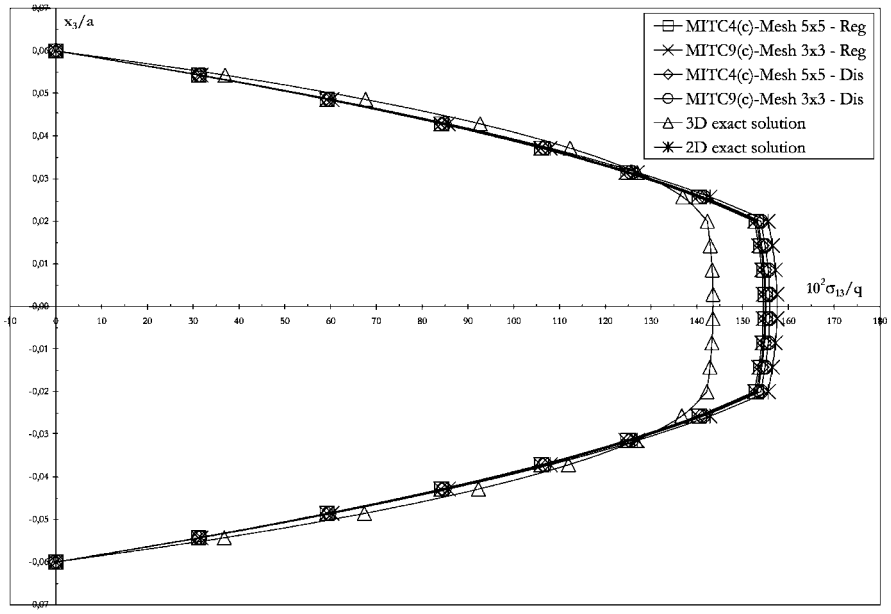

Figure 9. Through-the-thickness distributions of stress σ_{13} at $x = y = a/4$; Laminate 0/90/0.

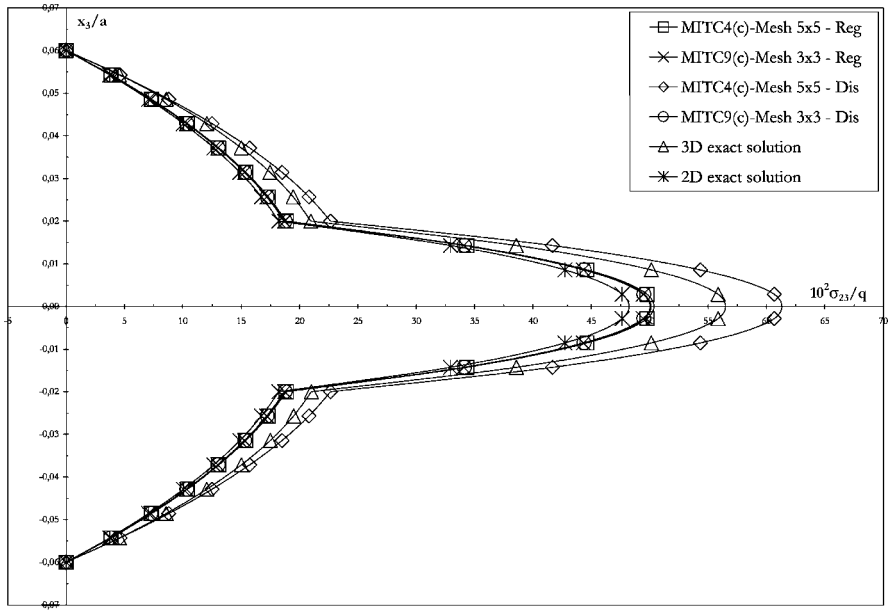

Figure 10. Through-the-thickness distributions of stress σ_{23} at $x = y = a/4$; Laminate 0/90/0.

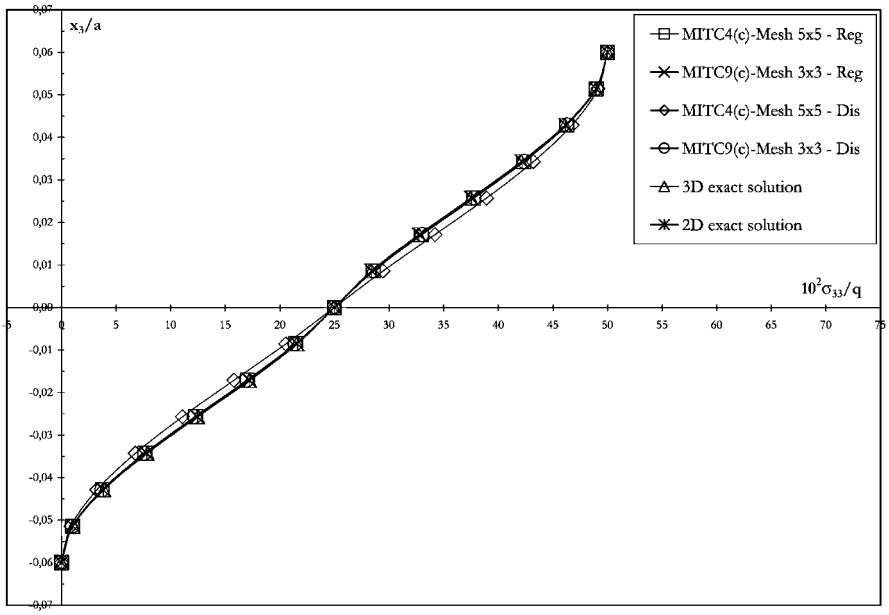

Figure 11. Through-the-thickness distributions of stress σ_{33} at $x = y = a/4$; Laminate 0/90.

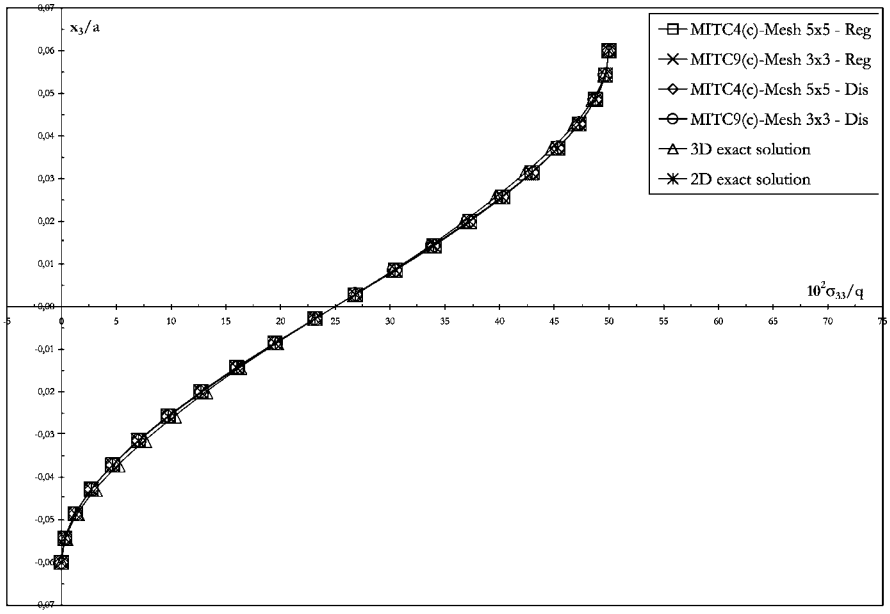

Figure 12. Through-the-thickness distributions of stress σ_{33} at $x = y = a/4$; Laminate 0/90/0.

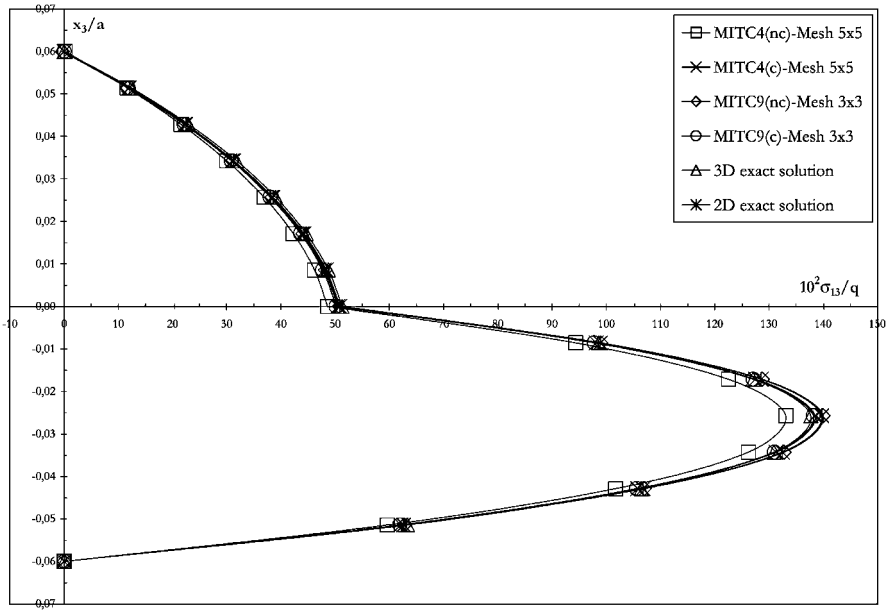

Figure 13. Through-the-thickness distributions of corrected (c) and non-corrected (nc) stress σ_{13} at $x = y = a/4$; Laminate 0/90, regular mesh.

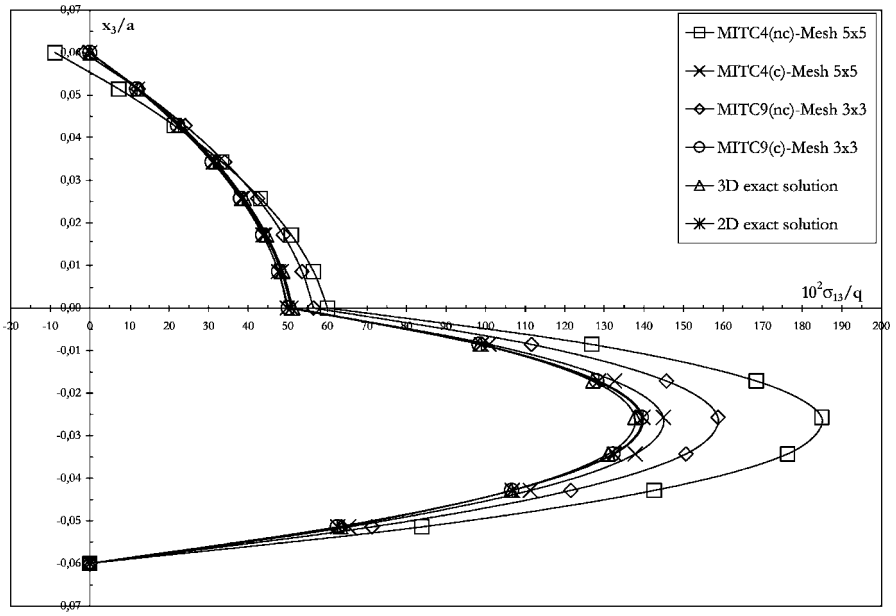

Figure 14. Through-the-thickness distributions of corrected (c) and non-corrected (nc) stress σ_{13} at $x = y = a/4$; Laminate 0/90, distorted mesh.

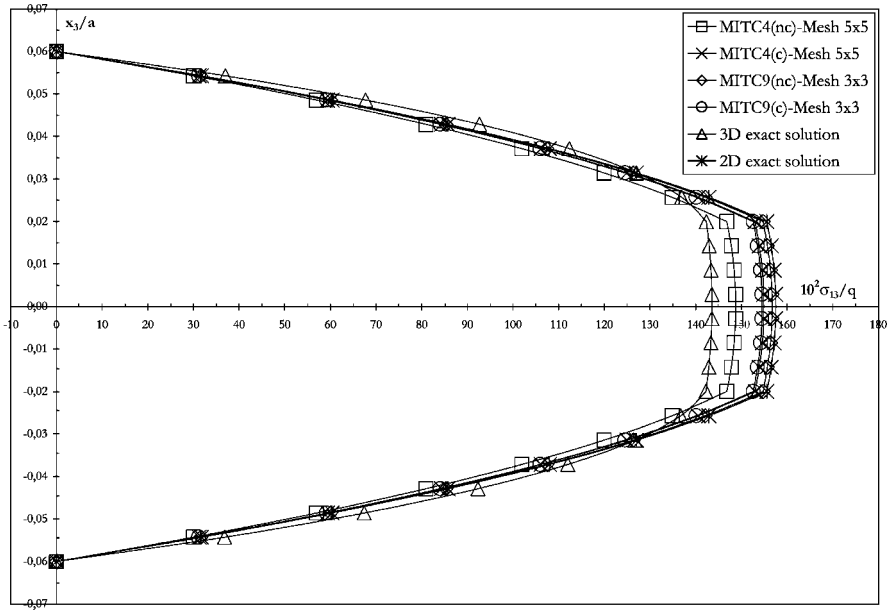

Figure 15. Through-the-thickness distributions of corrected (c) and non-corrected (nc) stress σ_{13} at $x = y = a/4$; Laminate 0/90/0, regular mesh.

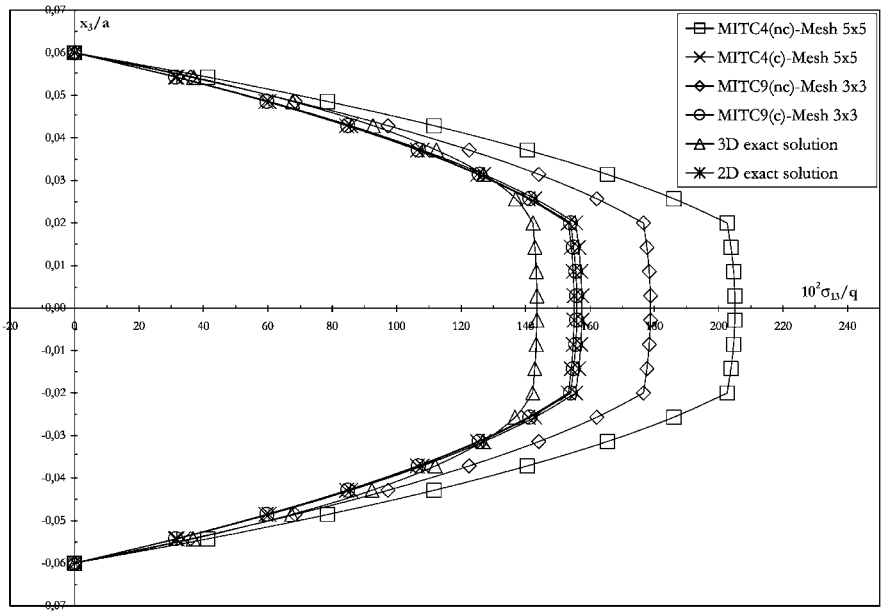

Figure 16. Through-the-thickness distributions of corrected (c) and non-corrected (nc) stress σ_{13} at $x = y = a/4$; Laminate 0/90/0, distorted mesh.

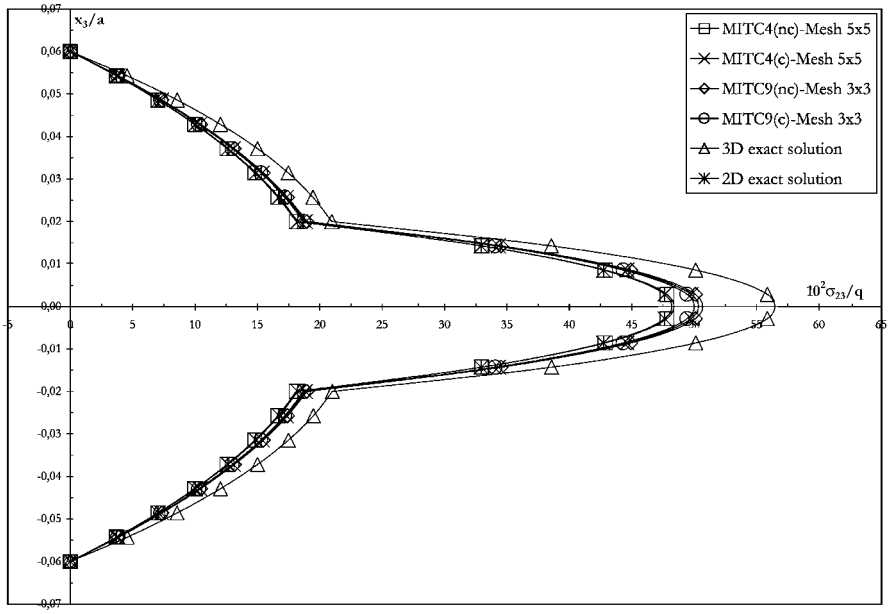

Figure 17. Through-the-thickness distributions of corrected (c) and non-corrected (nc) stress σ_{23} at $x = y = a/4$; Laminate 0/90/0, regular mesh.

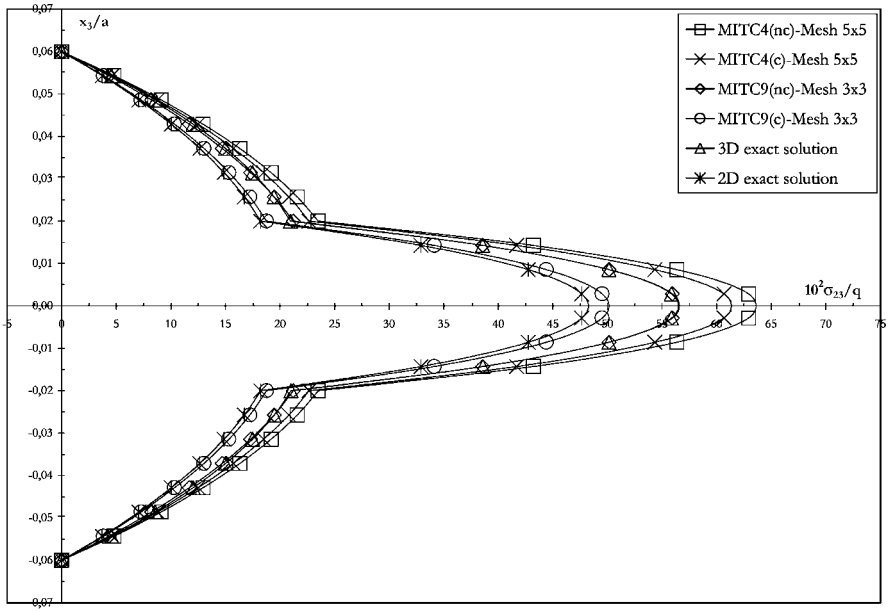

Figure 18. Through-the-thickness distributions of corrected (c) and non-corrected (nc) stress σ_{23} at $x = y = a/4$; Laminate 0/90/0, distorted mesh.

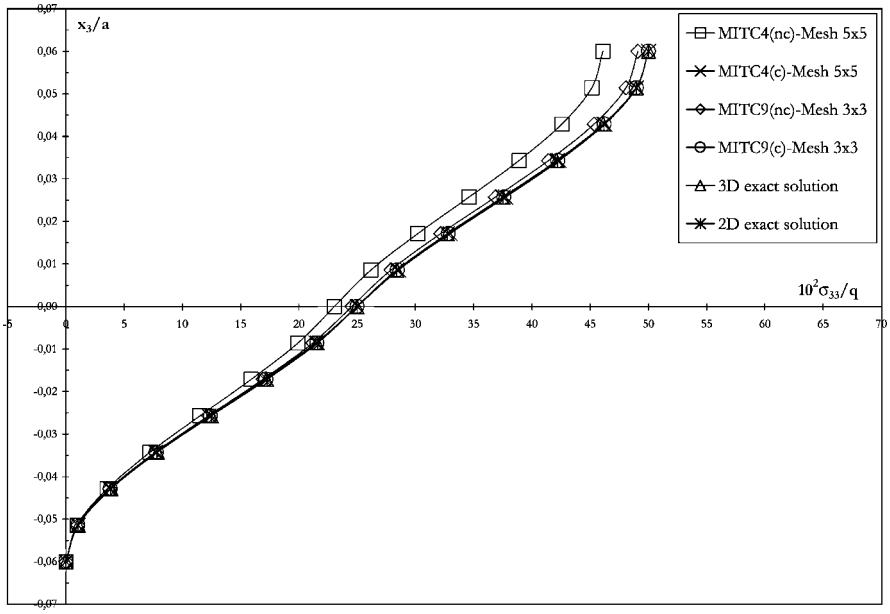

Figure 19. Through-the-thickness distributions of corrected (c) and non-corrected (nc) stress σ_{33} at $x = y = a/4$; Laminate 0/90, regular mesh.

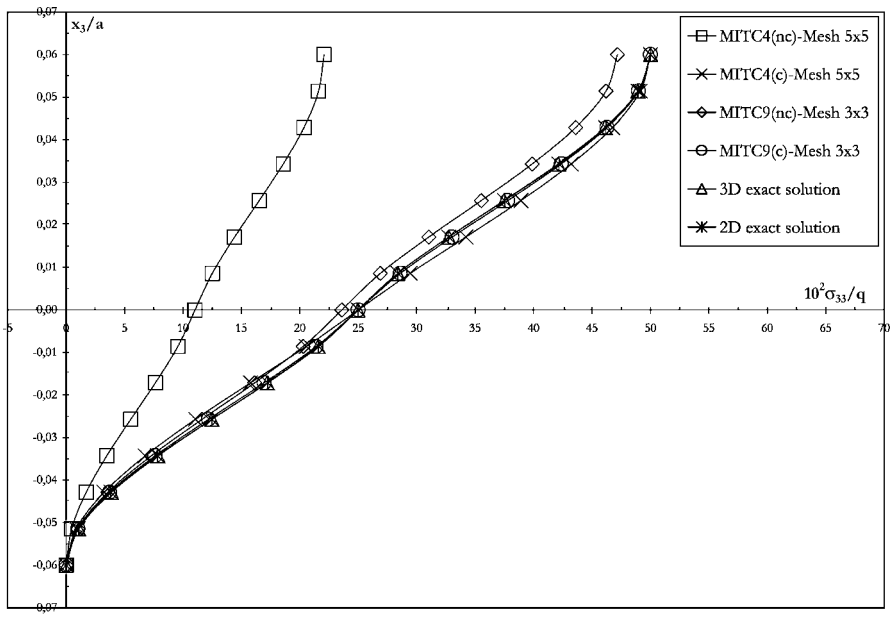

Figure 20. Through-the-thickness distributions of corrected (c) and non-corrected (nc) stress σ_{33} at $x = y = a/4$; Laminate 0/90, distorted mesh.

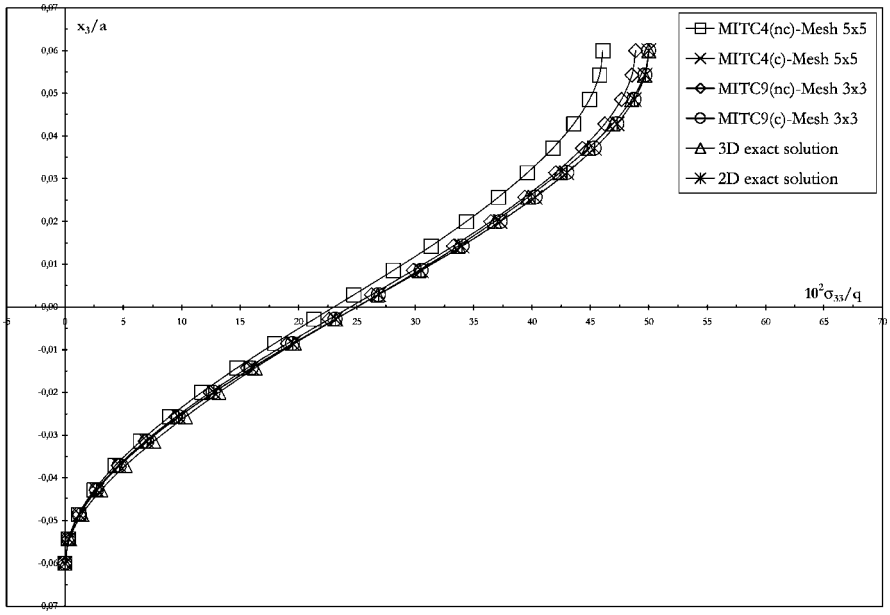

Figure 21. Through-the-thickness distributions of corrected (c) and non-corrected (nc) stress σ_{33} at $x = y = a/4$; Laminate 0/90/0, regular mesh.

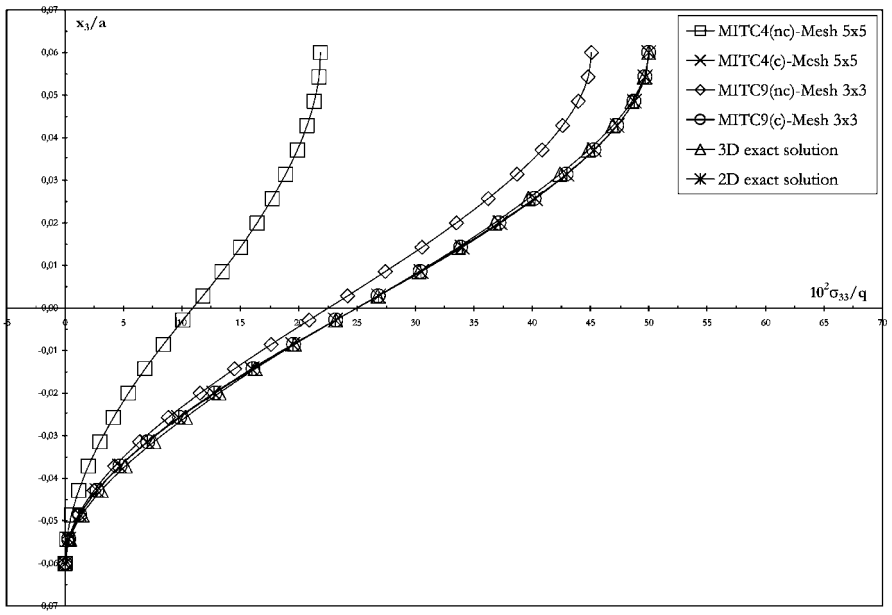

Figure 22. Through-the-thickness distributions of corrected (c) and non-corrected (nc) stress σ_{33} at $x = y = a/4$; Laminate 0/90/0, distorted mesh.

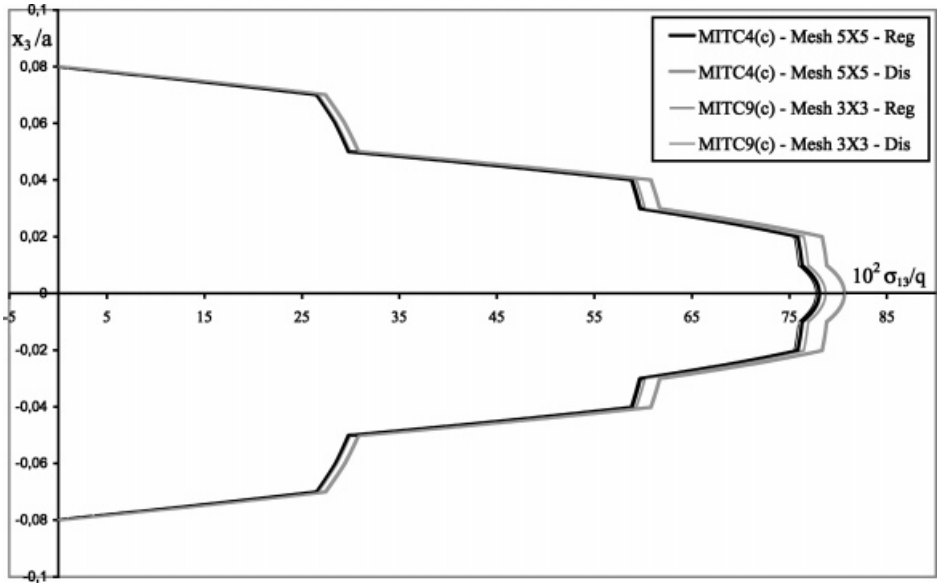

Figure 23. Through-the-thickness distributions of corrected (c) stress σ_{13} at $x = y = a/4$ for regular (Reg) and distorted (Dis) meshes; Laminate $(0/90/-45/45/-45/45/90/0)_{\text{sym}}$.

The results of Figures 13–22 are further elaborated upon in Figures 23 and 24, referred in turn to regular and distorted meshes, by plotting the correction procedure error ($c\,pe$) conventionally defined as follows:

$$\text{cpe} = \frac{\displaystyle\int_{-h/2}^{h/2} (\Delta\sigma)^2 \, \mathrm{d}x_3}{\displaystyle\int_{-h/2}^{h/2} \sigma^2 \, \mathrm{d}x_3}$$

both for the shear and normal out-of-plane stresses. In the previous formula σ denotes the exact value of the out-of-plane stress of the two-dimensional theory and $\Delta\sigma$ the difference between the finite element solution and the exact one provided by in turn by (60) and (61) for the shear stresses and by (62) and (63) for the normal stress.

A comparative examination of Tables I–II and Figures 13–22 shows that the error associated with the recovery of the out-of-plane stresses through the three-dimensional equilibrium equations is usually negligible and almost completely compensated by the proposed correction procedure. Further, the cpe value for regular meshes is two orders of magnitude lower than the one which characterizes the distorted ones. Finally, for both kinds of meshes, the cpe value for the MITC9 is one order of magnitude lower than the one pertaining to the MITC4 and, as was to be expected, by far more pronounced for the normal stress than for the shear stresses.

Furthermore, the comparisons reported in Figures 8–22, between the finite element solution and the exact analytical 3D one, appear to be particularly satisfactory. It can be emphasized that this kind of comparison is by far preferable with respect to other 3D numerical solutions which require a heavy computational burden and not necessarily provide a satisfactory solution.

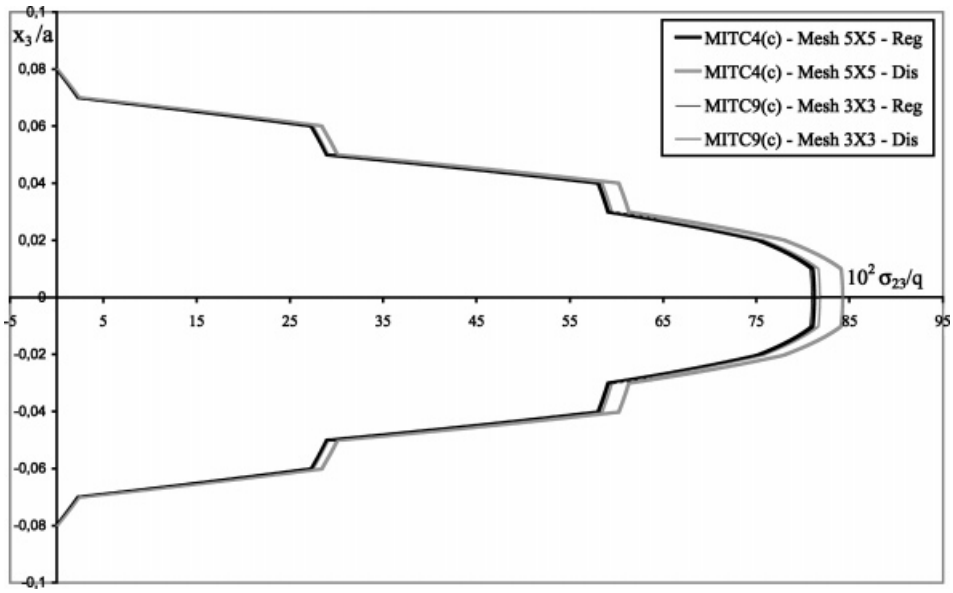

Figure 24. Through-the-thickness distributions of corrected (c) stress σ_{23} at $x = y = a/4$ for regular (Reg) and distorted (Dis) meshes; Laminate $(0/90/-45/45/-45/45/90/0)_{\text{sym}}$.

Table I. Correction procedure error (cpe) for the out-of-plane stresses; regular mesh.

	Laminate 0/90		Laminate 0/90/0	
	MITC4 - Mesh 5×5	MITC9 - Mesh 3×3	MITC4 - Mesh 5×5	MITC9 - Mesh 3×3
σ_{13}	$1.467E^{-3}$	$1.59E^{-4}$	$1.571E^{-3}$	$2.06E^{-4}$
σ_{23}	$1.623E^{-3}$	$2.41E^{-4}$	$1.518E^{-3}$	$1.75E^{-4}$
σ_{33}	$6.370E^{-3}$	$3.50E^{-4}$	$6.163E^{-3}$	$5.05E^{-4}$

Table II. Correction procedure error (cpe) for the out-of-plane stresses; distorted mesh.

	Laminate 0/90		Laminate 0/90/0	
	MITC4 - Mesh 5×5	MITC9 - Mesh 3×3	MITC4 - Mesh 5×5	MITC9 - Mesh 3×3
σ_{13}	$7.5090E^{-2}$	$1.8376E^{-2}$	$1.01909E^{-1}$	$2.1436E^{-2}$
σ_{23}	$1.30312E^{-1}$	$2.2754E^{-2}$	$2.010E^{-3}$	$1.6501E^{-2}$
σ_{33}	$3.25479E^{-1}$	$3.339E^{-3}$	$3.15343E^{-1}$	$9.637E^{-3}$

In order to evaluate the predicting capabilities of the proposed element for more complex cases we consider the stacking sequence $(0/90/-45/45/-45/45/90/0)_{\text{sym}}$.

The calculations refer to regular and distorted 3×3 and 5×5 meshes by using the 9- and 4-node MITC elements, respectively. Figures 23–25 show the shear stresses and the normal stress profiles. It is apparent that both the regular and distorted meshes provide similar results.

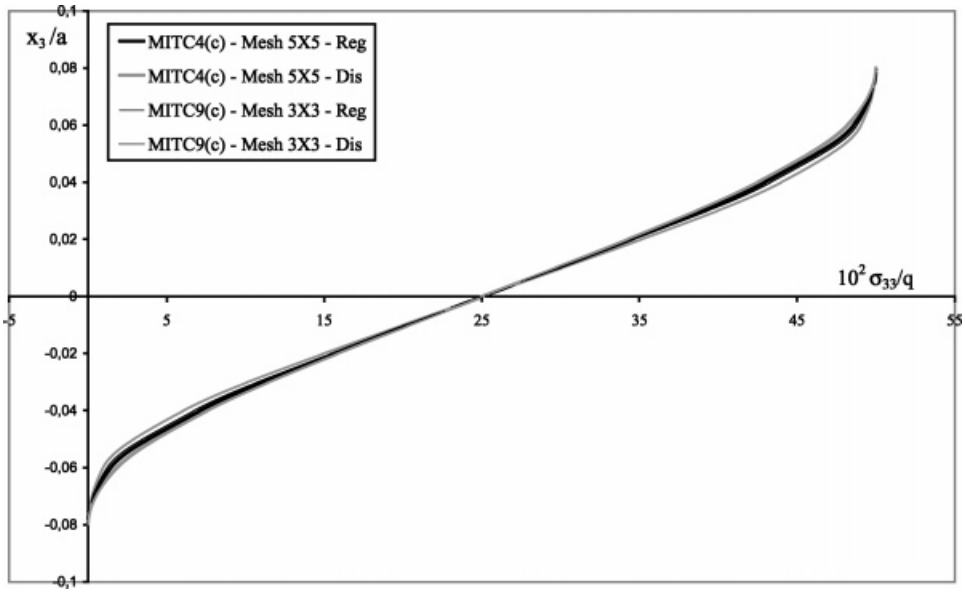

Figure 25. Through-the-thickness distributions of corrected (c) stress σ_{33} at $x = y = a/4$ for regular (Reg) and distorted (Dis) meshes; Laminate $(0/90/-45/45/-45/45/90/0)_{\mathrm{sym}}$.

As a final remark we note that both the 4- and 9-node proposed elements provide satisfactory out-of-plane stress profiles, also for distorted meshes. In particular, for meshes having the same number of nodes, the 9-node element behaves better than the 4-node one.

7. CONCLUSIONS

The excellent performances of the 4- and 9-node plate elements belonging to the MITC family [22–24], well known in the literature for the analysis of homogeneous plates, have been shown to carry over also to the case of composite laminates, both for the in-plane and transverse behaviour, within a FSDT framework.

The derived elements are locking free and allow a very accurate evaluation of the out-of-plane stresses, usually a delicate point in the FSDT, especially when coupled with the correction procedures of the stress profiles which have been presented in the paper.

The first one, which refers to the correction of the shear stresses, is a viable alternative to the one proposed in Reference [19] while the second one turned out to be very effective for the correct estimate of the normal stresses. This last result is particularly remarkable for the analysis of delamination effects in composites.

The effectiveness of the proposed approach in the evaluation of the stress state in laminated composite plates has been validated by the very satisfactory agreement of the closed-form solutions with the numerical results obtained either with regular and distorted meshes.

ACKNOWLEDGEMENTS

The financial support of the National Council of Research (CNR) and the Italian Ministry of University and Research (MURST) are gratefully acknowledged.

REFERENCES

1. Reddy JN. On refined theories of composite laminates. *Meccanica* 1990; **25**:230–238.
2. Reddy JN. A generalization of two-dimensional theories of laminated plates. *Communications in Applied Numerical Methods* 1987; **3**:173–180.
3. Reissner E. The effect of transverse shear deformation on the bending of elastic plates. *Journal of Applied Mechanics* 1945; **12**:69–77.
4. Mindlin RD. Influence of rotatory inertia and shear on flexural motions of isotropic, elastic plates. *Journal of Applied Mechanics* 1951; **38**:31–38.
5. Yang PC, Norris CH, Stavsky Y. Elastic wave propagation in heterogeneous plates. *International Journal of Solids and Structures* 1996; **2**:665–684.
6. Whitney JM, Pagano NJ. Shear deformation in heterogeneous anisotropic plates. *Journal of Applied Mechanics Transactions of ASME* 92/E 1970; **37**:1031–1036.
7. Seide P. An improved approximate theory for the bending of laminated plates. *Mechanics Today* 1980; **5**:451–466.
8. Di Sciuva M. Bending, vibration and buckling of simply supported thick multilayered orthotropic plates: an evaluation of a new displacement model. *Journal of Sound and Vibration* 1986; **105**:425–442.
9. Di Sciuva M. An improved shear deformation theory for moderately thick multi-layered anisotropic shells and plates. *Journal of Applied Mechanics* 1987; **54**:589–596.
10. Barbero EJ, Reddy JN. An accurate determination of stresses in thick laminates using a generalized plate theory. *International Journal for Numerical Methods in Engineering* 1990; **29**:1–14.
11. Carrera E. Evaluation of layerwise mixed theories for laminated plate analysis. *AIAA Journal* 1998; **36**(5):830–839.
12. Robbins Jr DH, Reddy JN. Modelling of thick composites using a layerwise laminate theory. *International Journal for Numerical Methods in Engineering* 1993; **36**:655–677.
13. Gaudenzi P, Mannini A, Carbonaro R. Multi-layer higher order finite elements for the analysis of free-edge stresses in composite laminates. *International Journal for Numerical Methods in Engineering* 1998; **41**:851–873.
14. Zienkiewicz OC, Taylor RL, Too JM. Reduced integration techniques in general analysis of plates and shells. *International Journal for Numerical Methods in Engineering* 1971; **3**:275–290.
15. Zienkiewicz OC, Taylor RL. *The Finite Element Method*, vols. I, II. McGraw Hill: New York, 1991.
16. Malkus DS, Hughes TJR. Mixed finite-element methods—reduced integration techniques: a unification of concepts. *Computer Methods in Applied Mechanics and Engineering* 1978; **15**:63–81.
17. Pugh EDL, Hinton E, Zienkiewicz OC. A study of quadrilateral plate bending elements with reduced integration. *International Journal for Numerical Methods in Engineering* 1978; **12**:1059–1079.
18. Auricchio F, Taylor RL. A shear-deformable plate element with an exact thin limit. *Computer Methods in Applied Mechanics and Engineering* 1994; **118**:393–412.
19. Auricchio F, Sacco E. A mixed-enhanced finite-element for the analysis of laminated composite plates. *International Journal for Numerical Methods in Engineering* 1999; **44**:1481–1504.
20. Pagano NJ. Exact solutions for rectangular bidirectional composites and sandwich plates. *Journal of Composite Materials* 1970; **4**:20–34.
21. Simo JC, Rifai MS. A class of mixed assumed strain methods and the method of incompatible modes. *International Journal for Numerical Methods in Engineering* 1990; **29**:1595–1638.
22. Bathe KJ, Dvorkin EN. A four-node plate bending element based on Mindlin/Reissner plate theory and a mixed interpolation. *International Journal for Numerical Methods in Engineering* 1985; **21**:367–383.
23. Bathe KJ, Dvorkin EN. A formulation of general shell elements. The use of mixed interpolation of tensorial components. *International Journal for Numerical Methods in Engineering* 1986; **22**:697–722.
24. Bucalem ML, Bathe KJ. Higher-order MITC general shell elements. *International Journal for Numerical Methods in Engineering* 1993; **36**:3729–3754.
25. Guillermin O, Kojic M, Bathe KJ. Linear and nonlinear analysis of composite shells. *Proceedings of STRUCOME 90, DATAID AS & I*, Paris, 1990.
26. Auricchio F, Sacco E. Partial mixed formulation and refined models for the analysis of composite laminates within a FSDT. *Composite and Structures* 1999; **46**:103–113.
27. Bisegna P, Sacco E. A rational deduction of plate theories from the three-dimensional linear elasticity. *Zeitschrift für Angewandte Mathematik und Mechanik* 1997; **77**:349–366.
28. Noor AK, Burton WS, Peters JM. Predictor-corrector procedures for stress and free-vibration analyses of multylayered composite plates and shells. *Computer Methods in Applied Mechanics and Engineering* 1990; **82**:341–363.
29. Brezzi F, Bathe KJ, Fortin M. Mixed interpolated elements for Reissner-Mindlin plates. *International Journal for Numerical Methods in Engineering* 1989; **28**:1787–1801.
30. Reddy JN. *Energy and Variational Methods in Applied Mechanics.* Wiley: New York, 1984.

